December 2020

Temperature Effects on Rate of Trichloroethene Degradation in Fractured Sandstone Using a 14C-Assay

Bethany Ann Byrd
Clemson University, babyrd@clemson.edu

TEMPERATURE EFFECTS ON RATE OF TRICHLOROETHENE DEGRADATION IN FRACTURED SANDSTONE USING A ^{14}C-ASSAY

A Thesis
Presented to
the Graduate School of
Clemson University

In Partial Fulfillment
of the Requirements for the Degree
Master of Science
Environmental Engineering and Earth Sciences

---

by
Bethany A. Byrd
December 2020

Accepted by:
Dr. David L. Freedman, Committee Chair
Dr. Kevin T. Finneran
Dr. Cindy M. Lee

ABSTRACT

Abiotic and biologically mediated abiotic degradation of chlorinated ethenes has been documented at many sites. One of the challenges with relying on this mechanism is slow rates. A simple way to enhance the rates is to heat the subsurface, e.g., using borehole heat exchangers powered by solar photovoltaics. Raising the groundwater temperature by ~5 to 20°C has the potential to increase abiotic and biotic rates to an extent that will significantly reduce remediation times and/or the extent of a contaminant plume. The objective of this study was to assess the effect of heating on degradation of trichloroethene (TCE) using samples of crushed sandstone rock and groundwater.

A ^{14}C-TCE assay was developed to determine pseudo first-order rate coefficients for the degradation of TCE based on a crushed rock microcosm study. The assay involved the development of a first-order model that determined rate coefficients based on product accumulation while accounting for volumetric changes in the serum bottles due to sampling and corresponding changes to the distribution of TCE between the aqueous and gaseous phases. Results proved that increasing temperature subsequently increases the rate of TCE degradation by a factor of 1.3 in the unamended treatment and a factor of 2.6 in the lactate-amended treatment. These results come from increasing the temperature from ambient groundwater temperature 18°C to 30°C.

TABLE OF CONTENTS

LIST OF FIGURES

LIST OF TABLES

ABBREVIATIONS & ACRONYMS

BMAD	biologically mediated abiotic degradation
cDCE	*cis*-1,2-dichloroethylene
CO_2	carbon dioxide
DDI	distilled deionized
Dhc	Dehalococcoides
dpm	disintegrations per minute
FID	flame ionization detector
FSGW	filter-sterilized groundwater
GC	gas chromatograph
HCl	hydrochloric acid
ISTR	in-situ thermal remediation
LSC	liquid scintillation cocktail
MNA	monitored natural attenuation
NaOH	sodium hydroxide
NSR	non-strippable residue
PCE	tetrachloroethylene
PTFE	polytetrafluoroethylene
TCE	trichloroethylene
VC	vinyl chloride
VOC	volatile organic compound

1.0 INTRODUCTION

Chlorinated ethenes are among the most frequently detected groundwater pollutants in the United States due to expansive use as degreasers in the years leading up to the 1980s.[1] Understanding of the degradation pathways of chlorinated ethenes is crucial in the context of implementing remediation strategies, especially in consideration of which strategy to use. Monitored natural attenuation (MNA) is a remediation strategy that considers the total contributions of natural biotic and abiotic processes, such as biodegradation, sorption, dilution and volatilization, among others, that lead to contaminant remediation over time.[2] MNA continues to grow in popularity as a remediation strategy due to its relatively low cost and low environmental impact. The most relevant disadvantages include the extended time frame needed to achieve acceptable contaminant level reduction, potential for reductive dechlorination to "stall-out" leaving more hazardous byproducts (e.g., vinyl chloride (VC) from reductive dechlorination of trichloroethene (TCE)) and the inability to reduce significantly high concentrations of contaminants to target levels. To be considered for a remedial action plan, MNA must be clearly demonstrated for an individual site. In 1997, the Office of Solid Waste and Emergency Response Directive 9200.4-17 identified three lines of evidence to demonstrate MNA: 1) historical groundwater and/or soil chemistry data (primary); 2) hydrogeological and geochemical data (secondary); and 3) field or microcosm studies (tertiary).[3]

The research presented in this thesis investigated the effect of temperature on the rate of natural attenuation, specifically degradation of TCE at an industrial site where the fractured sandstone contains a substantial level of the contaminant within the rock matrix.

The degradation of chlorinated solvents, such as TCE, has been widely studied at the site through various microcosm studies, which provides a third line of evidence that natural attenuation is occurring. Degradation has been discovered to occur via abiotic and biotic pathways.[4–7] Previous microcosm studies utilizing groundwater and crushed rock from the industrial site indicate that degradation of TCE and possibly *cis*-1,2-dichloroethene (cDCE) may be enhanced by addition of an electron donor such as lactate.[6,7] The goal of enhanced natural attenuation is to increase the rate of TCE degradation to environmentally acceptable endpoints such as ethene, ethane, acetylene, carbon dioxide (CO_2), and volatile acids.

Figure 1 summarizes the biotic and abiotic anaerobic pathways that have been documented for dechlorination of tetrachloroethene (PCE) and TCE. The dominant biotic pathway occurs through hydrogenolysis, whereby the chlorines on PCE and TCE are removed sequentially, yielding cDCE, VC, ethene, and ethane. Alternatively, PCE and TCE can abiotically undergo β-elimination to dichloroacetylene and chloroacetylene, respectively. Chloroacetylene undergoes hydrolysis to acetic acid or reduction to acetylene.[5,8–10] Acetylene is subsequently reduced to ethene or may undergo fermentation to acetaldehyde and acetic acid by acetylenotrophs.[10] Through the use of ^{14}C-labeled TCE and cDCE, previous studies have also demonstrated anaerobic conversion of TCE and cDCE to soluble products that are non-volatile (identified as non-strippable reside (NSR)), as well as oxidation to CO_2. The experimental design for this research allows for quantification of TCE and cDCE degradation via the various pathways shown in Figure 1.

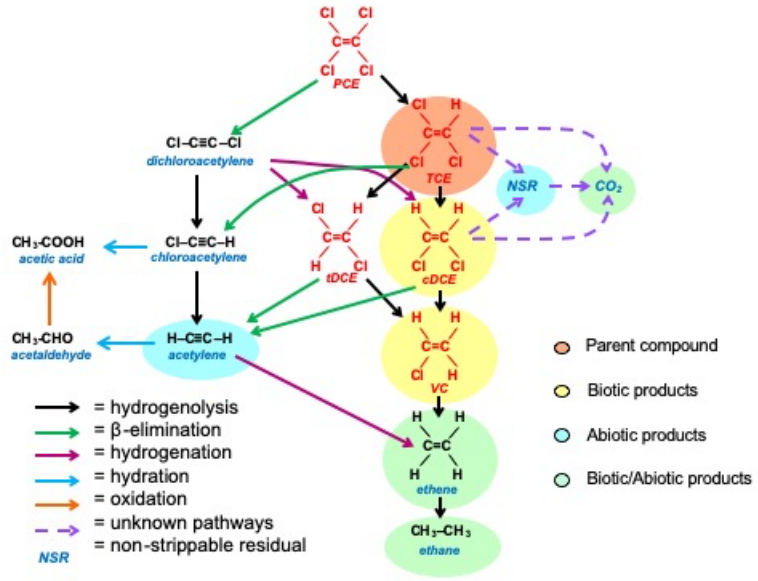

Figure 1. Anaerobic biotic and abiotic pathways for degradation of chlorinated ethenes.[11]

Understanding the degradation pathways of chlorinated ethanes and ethenes in groundwater is crucial in the context of implementing a remediation strategy. Since remediation techniques are expensive and are frequently invasive, natural attenuation is often considered a cost effective but longer-term technique. Understanding natural attenuation mechanisms enables one to choose which sites need remediation and which can be left to decrease naturally.[12]

The effect of temperature on anaerobic biotic TCE dechlorination has been studied extensively, e.g., with a highly enriched *Dehalococcoides (Dhc)*-containing culture that received lactate or propionate as electron donors.[13] Complete TCE reduction to ethene occurred in the range of 10-30°C for lactate-amended and 15-30°C for propionate amended. Highest growth rates on TCE were observed in the lactate-amended group at 30°C, with a rate constant of 7.00±0.14 d^{-1}, confirming a strong temperature dependence.

The rate at 20°C was approximately 60% lower than that of 30°C, and the rate at 40°C was approximately 70% lower than 30°C.[13] Biotic degradation via the addition of electron donors can accelerate the rate of reductive dechlorination, often in conjunction with the addition of microbial cultures, such as *Dhc*, which is the predominant microbe observed to reduce PCE and TCE to ethene.[14] *Dehalogenimonas* are also known to accomplish complete dechlorination via organohalide respiration. Yang et al.[15] describe a microcosm study in which grape pomace compost and derived solid-free enrichment cultures successfully dechlorinated TCE to cDCE and ethene where *Dhc* biomarker genes were not detected based on 16S rRNA gene amplicon and qPCR analyses. It is known that the temperature range for growth of strain *Dehalogenimonas alkenigignens* (IP3-3), a strictly anaerobic bacterium, is between 18-42°C, with optimum performance between 30-34°C.[16]

Hu et al.[17] conducted a study on the effect of nutrients on the anerobic degradation of TCE at optimal temperature. The UC-1 culture, enriched with TCE as the electron acceptor and lactate as the electron donor, showed complete degradation of TCE at 35°C and the TCE degradation rate increased with increasing temperature up to 35°C.

While studies focusing specifically on the effect of temperature on abiotic degradation of TCE are lacking, there are numerous studies on the effects of various electron donors at temperatures ranging from 14 to 35°C, which falls within the temperature range of this study.[18–21] Simulations in a feasibility study of thermal in situ bioremediation found that by increasing the groundwater temperature from 15 to 35°C, the amount of mass not degraded in situ was reduced by 94%. Remediation time frames were

also predicted to be reduced by 70%.[22] The data resulting from this thesis provide insight into how temperature specifically affects rates of degradation in TCE.

In situ thermal remediation (ISTR) has been increasingly deployed over the past two decades as a way to enhance degradation of contaminants. While the focus of this thesis is on modest increases in temperature (i.e., up to ~20ºC above ambient), ISTR extends as far as increasing subsurface temperatures to the boiling point, in order to induce volatilization due to increases in vapor pressure and Henry's Law constants.[23]

The use of ^{14}C-TCE in this thesis made it possible to track degradation products in addition to volatiles. Microcosms were prepared under anaerobic conditions and placed in temperature-controlled incubators ranging from 18-40°C. The lower temperature represented average ambient conditions at the industrial site and the upper temperature represented the highest projected increase that is attainable using solar panels to provide the energy for heating.

When considering the contribution of microbial activity to biologically mediated abiotic degradation (BMAD), it is important to note the significance of the temperature range chosen. This study focused on microbial activity in the mesophilic range, meaning the organisms were adapted to moderate temperatures (i.e., ~20 to 40°C), with a peak around 30°C (Figure 2).

Methods to document the rate of in situ reductive dechlorination of TCE, as well the quantity of microbes and enzymes involved, are well-established.[14,25–30] Quantification of biotic and abiotic degradation using ^{14}C-labeled compounds has been in use for decades, and numerous studies have employed ^{14}C-TCE.[4,7,31–33] Nevertheless, an analysis of the

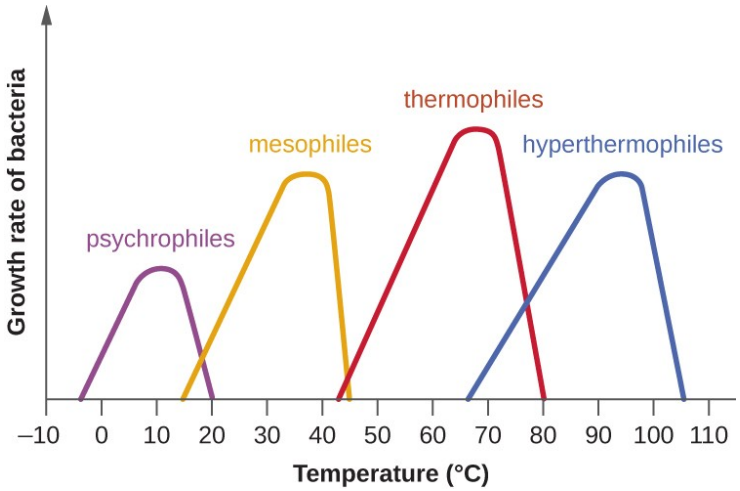

Figure 2. The growth rate of microbes as a function of temperature.[24]

effect of low temperature heating, i.e., controlled heating in a low range, on abiotic dechlorination based on product formation from ^{14}C-TCE is lacking. By measuring the accumulation of ^{14}C-labeled products from ^{14}C-TCE degradation, Mills et al.[34] demonstrated it was possible to measure first order rate constants that equate to half-lives even in excess of 100 years.

The objective of this research was to study the effects of small, low temperature increases and biostimulation on TCE degradation rates in fractured sandstone. TCE that back-diffuses from sandstone poses a potential ongoing groundwater contamination source as groundwater moves through fractures in the rock. Since excavation or pumping and treating are not effective long-term remediation strategies for this undisclosed site, other approaches such as MNA or enhanced MNA should be considered. One way to achieve enhanced MNA is through addition of electron donor, referred to as biostimulation. Both processes may benefit by a modest increase in the temperature of the subsurface, since the

rate of biotic and abiotic processes usually improve at higher temperatures, which are still low enough to avoid denaturing of enzymes and other proteins.

2.0 MATERIALS AND METHODS

2.1 Experimental Design

Microcosms were prepared in 160 mL serum bottles according to the treatments outlined in Table 1. Each treatment was conducted in triplicate at 18, 25, 30, 35, and 40°C, totaling 60 microcosms. The lowest temperature represents the median for groundwater at the site where ISTR is being considered. The highest temperature projected in response to heating is 40°C. Microcosms were incubated for six months, to allow sufficient data collection for calculating a pseudo first order rate constant. The rate constants were then used to determine Arrhenius constants.

Table 1. Experimental design.

Treatment	Purpose	Amendment
Unamended (UN)	Assess in situ conditions	--
Killed Control (KC)	Assess abiotic degradation	$HgCl_2$
Lactate-Amended (LAC)	Assess effect of biostimulation	Sodium lactate syrup
Filter Sterilized Ground Water (FSGW)	Assess the background level of abiotic activity in the absence of the rock	--

2.2 Site location and sample collection

Geology analyses of the site concludes it is underlain with material, Chatsworth formation, consisting of interbedded sandstone and shale. It is believed this was deposited by marine turbidites, uplifted during the Upper Cretaceous.[5,35] Samples of crushed rock were obtained from the University of Guelph. Rock cores were collected from a source

zone (borehole C-19) contaminated with TCE. The rock, sandstone, was then crushed, placed in metalized vacuum bags, sealed under anoxic conditions, and refrigerated. Groundwater was obtained from the nearest monitoring well and shipped on ice along with the crushed rock samples to Clemson University. The rock and groundwater were stored at 4°C until use.

2.3 Chemicals

^{14}C-TCE (1.0 mCi) was custom-synthesized by Moravek Biochemicals, Inc. (Brea, CA, USA) and dissolved in acetonitrile. The specific activity was 60 mCi/mmol and the radiochemical purity was at least 97%. A stock solution was prepared in a glass 65 mL bottle by adding the ^{14}C-TCE/acetonitrile solution to ~60 mL of TCE (99.5%, Aldrich) saturated distilled deionized (DDI) water (~8.6 μmol TCE/mL) to reduce the specific activity of the ^{14}C-TCE. The bottle was sealed with a Mininert valve and stored at 10°C. *cis*-1,2-DCE (99%) was obtained from TCI America; methane (99.99%), ethane (99.99%), acetylene (99%), and VC (<1 ppm of nitrogen) from Matheson; and ethene (99.5%) from National Welders. Ultima Gold™ XR (Perkin Elmer) was used in liquid scintillation counting. NaOH (ACS grade) pellets was obtained from AMRESCO, and HCl (ACS grade) from Aristar.

2.4 ^{14}C-TCE purification and addition

Following procedures outlined by Mills et al.,[34] ^{14}C-TCE was separated from the acetonitrile and impurities in the stock solution on a gas chromatograph (HP 5890 Series II). An aliquot of the stock solution (50 μL) was injected (100 μL liquid syringe; VICI, Series C) onto a stainless-steel column (2.44 m x 3.175 mm) packed with 1% SP-1000 on

60/80 Carbopack-B (Supelco). The end of the column was connected to a four-port valve in the GC oven. The valve was positioned so that the flow exited the oven through stainless-steel tubing (1.59 mm) rather than routing to the flame ionization detector (FID). The tubing terminated with a threaded Luer-Lok™ fitting for attachment of a sterile needle, through which the purified ^{14}C-TCE was injected at a predetermined residence time into the serum bottles. Prior to injecting the purified ^{14}C-TCE, 25 mL of headspace was withdrawn with a 25 mL gas-tight syringe (SGE, removable Luer-Lok™) to compensate for the gas being added, so that the headspace was not over pressurized.

High purity N_2 served as the carrier gas (33.5 ± 0.5 mL/min). The temperature program was 60°C for 2 min, increased at 20°C per min to 150°C, increased at 10°C to 200°C and held for 38.5 min. The elution time for TCE was 10.15-10.75 min. The average amount of ^{14}C-TCE added to the serum bottles was approximately 0.380 μCi (840,000 disintegrations per minute (dpm)). The extended hold time at 200 °C was designed to ensure that impurities did not accumulate on the column.[34] After every six injections, the column was checked for residual impurities by following the above protocol, with the exception of injecting 50 μL DDI water onto the GC. At the retention time when TCE elutes (Appendix A.1, Table A.1), the carrier gas was injected into a serum bottle containing 100 mL of DDI water. Headspace and liquid samples (described below) from the serum bottle were analyzed to determine the amount of remaining radioactive impurities eluting from the column. If the ^{14}C recovered exceeded 0.027 μCi/bottle (60,000 dpm), the column was held at 200°C until the level of ^{14}C recovered decreased. This threshold represents ~5.5% of the total ^{14}C added when injecting ^{14}C-TCE.

2.5 Microcosm preparation and time-zero measurements

Rock and groundwater samples were transferred to an anaerobic chamber. The double-sealed bags of anoxic crushed rock were opened and transferred to a sterile Tupperware container, where they were homogenized; the container was kept closed when not in use to limit volatilization of contaminants and moisture loss. Percent moisture and density analysis of the crushed rock was conducted (Appendix (A.2, Tables A.5 and A.6)

Triplicate microcosms were prepared for each treatment at each temperature inside the anaerobic chamber, which were then sealed with slotted gray butyl septa and aluminum crimp caps. The unamended, lactate-amended, and killed control microcosms received 12 g of crushed rock plus 100 mL of groundwater. The groundwater controls received 100 mL of FSGW. The groundwater was amended with resazurin, a redox indicator (1 mg/L). Microcosms were then removed from the anaerobic chamber and sparged with high purity N_2 for 60 s inside a fume hood to remove residual hydrogen remaining from the anaerobic chamber environment. The slotted gray butyl septa were replaced with PTFE-faced gray butyl septa and aluminum crimp caps and stored cap down to minimize diffusional losses. The microcosms were spiked with the ^{14}C-TCE as described above. Lactate-amended microcosms received 30 μmol per bottle sodium lactate syrup (0.1 mL of a 0.3 M stock solution)), resulting in an initial concentration of 0.30 mM. The killed control microcosms received 100 μmol per bottle $HgCl_2$ (1 mL of a 0.1 M stock solution), resulting in an initial concentration of 1.0 mM. Previous studies indicate using this concentration of $HgCl_2$ is sufficient to inhibit microbial activity.[36] It took approximately one week to prepare the 60 microcosms.

Immediately after constructing the microcosms, the bottles were inverted and placed on an orbital shaker table (200 RPM) for approximately 1 h to equilibrate the headspace and liquid phases. Headspace samples were evaluated for volatile organic compounds (VOCs) (section 2.7). Addition of ^{14}C-TCE resulted in an average time-zero TCE level of 0.260 μmol per bottle, or an aqueous phase concentration ranging from 239 μg/L at 40°C to 298 μg/L at 18°C, when taking into account partitioning between the headspace and liquid phases.[37]

Time-zero monitoring for ^{14}C involved measurement of dpm levels in the headspace and liquid. Direct sample counts were used to quantify the total amount of radioactive material in each bottle. Headspace samples (0.5 mL gas) were removed using a 1 mL gas-tight syringe. Liquid samples (100 μL) were removed using a 100 μL liquid syringe (VICI Series C). Samples were injected immediately into 20 mL borosilicate glass scintillation vials (Fisherbrand™) containing 15 mL of liquid scintillation cocktail (LSC). A hole (2.38 mm) was drilled in the polypropylene scintillation cap and a PTFE-faced gray butyl rubber septum was placed inside the cap to minimize any losses of ^{14}C from volatilization. The total amount of ^{14}C present per bottle was determined as follows.

$$C_{tot,i,m} = \frac{S_{h,i}}{V_{h,s}} \cdot V_{h,b} + \frac{S_{l,i}}{V_{l,s}} \cdot V_{l,b} \qquad (1)$$

where $C_{tot,i,m}$ = total ^{14}C activity in a serum bottle (dpm); $S_{h,i}$ = ^{14}C activity in a headspace sample (dpm); $V_{h,s}$ = volume of headspace sample (0.5 mL); $V_{h,b}$ = volume of headspace in a serum bottle (54 mL for the unamended, lactate-amended, and killed control microcosms; the rock displaced ~6 mL of volume; ~60 mL for the FSGW microcosms); $S_{l,i}$ = ^{14}C activity

in liquid sample (dpm); $V_{l,s}$ = volume of liquid sample (0.1 mL); and $V_{l,b}$ = volume of liquid in a serum bottle (~100 mL).

For alkaline and acid sparging, a 5 mL liquid sample was withdrawn, filtered (0.2 μm syringe filter) to remove particulates, and split into 2.5 mL subsamples placed in two scintillation vials (designated $V_{alkaline}$ and V_{acidic}). Approximately 12 μL of 8 M NaOH was added to $V_{alkaline}$ using a 100 μL liquid syringe (VICI Series C) to raise the pH above 10.5. Approximately 12 μL of 8 M HCl was added to V_{acidic} using a 100 μL liquid syringe (VICI Series C) to lower the pH below 3. The pH of the samples was confirmed qualitatively using pH strips (BDH® VWR Analytical, pH 0.0-7.0; 7.0-14.0, gradation of 0.5 units). Raising the pH above 10.5 ensured the retention of $^{14}CO_2$ and ^{14}C-NSR compounds in the aqueous phase; lowering the pH below 3 ensured the retention of only ^{14}C-NSR products. The acid and alkaline liquid samples were sparged with N_2 (550 ± 50 mL/min) for 30 min. The adequacy of this approach to remove ^{14}C-TCE was confirmed by checking for residual TCE by GC analysis of a headspace sample after sparging. The N_2 flow rate was controlled using air flow meters (Cole-Parmer, 1.4 LPM maximum) connected to latex rubber tubing that terminated in sparging needles (Cadence Science non-sterile hypodermic needle, 22 gauge). The vials were tilted on a 30-degree angle to facilitate contact between the N_2 and liquid (Appendix A.3, Figure A.2).

Following sparging of $V_{alkaline}$ and V_{acidic}, 15 mL of LSC was added to the vials, which were incubated quiescently in the dark for approximately 12 h before counting. The amount of $^{14}CO_2$ present was calculated based on the difference between $V_{alkaline}$ and V_{acidic}. The ^{14}C activity in V_{acidic} yielded the amount of ^{14}C-NSR.

After each microcosm was sampled, 6.1 mL of high-purity N_2 gas was injected into the serum bottles to replace the volume of the extracted samples and avoid creating a negative pressure in the headspace. A 10 mL gas-tight syringe was used for this purpose. The high purity N_2 was injected after passage through a titanium chloride solution to ensure no oxygen was introduced into the microcosms.

2.6 Monitoring and ^{14}C product distribution

Serum bottles were placed in their respective temperature-controlled incubators (VWR Personal Low Temp Incubator #89511-416) on the laboratory countertop (Appendix A.4, Figure A.3). Sampling occurred approximately every 14 days for 3-6 months. At each sampling event, headspace and liquid samples were counted to determine the total ^{14}C remaining and a headspace sample was used to measure the concentration of VOCs present. Aqueous phase product accumulation was determined in two 2.5 mL liquid samples (acid and alkaline), as described above. After each sampling of the lactate-amended microcosm, an additional 0.1 mL sodium lactate syrup was added to provide a consistent source of electrons throughout the incubation, totaling 0.9 mL per microcosm (0.27 mmol) by the end of incubation.

On the final day of incubation, routine measurements were made (i.e., ^{14}C remaining in the headspace and liquid, VOC levels, and ^{14}C products in two 2.5 mL liquid samples). To estimate the amount of ^{14}C that had adsorbed to the rock, a well-mixed sample from the serum bottle (groundwater and crushed rock) was withdrawn (5.0 mL) and equally split between $V_{alkaline}$ and V_{acidic} vials, without filtering. The contents were sparged for 30 min with high purity N_2 to remove ^{14}C-TCE from the aqueous phase. LSC was then added

to the vials, which were incubated overnight in the dark before counting the ^{14}C activity. The difference in activity between the vials with and without rock present was used to estimate the amount of adsorbed ^{14}C.

Adsorption of TCE to the crushed rock results in some of the TCE in the bottles partitioning out of the liquid phase, where it is no longer subject to removal when liquid samples were withdrawn. This impacts the mass balance on ^{14}C in the bottles, which keeps track of the amount of ^{14}C removed at each sampling point (see below). Since the extent of adsorption was estimated only at the end of the incubation period (i.e., the "slurry sample" procedure, Appendix A.5), hypotheses were made about the rate of adsorption throughout the incubation. One hypothesis was that adsorption occurred linearly, i.e., starting at zero adsorption on day zero and progressing at a linear rate through to the final sampling event, for which the percent adsorption was measured. The second hypothesis was that adsorption occurred at a non-linear rate (see below).

2.7 Analysis of VOCs and Response Factor Calculations

The amount of VOCs present was quantified by injection of a headspace sample (0.5 mL, taken with a 1.0 mL gas-tight syringe, VICI Series A-2) onto a GC (HP 5890 Series II) equipped with a stainless-steel column packed with 1% SP-1000 on 60/80 Carbopack B (Supelco) and FID, as described above. Before the initial ^{14}C-TCE addition, one microcosm from each treatment was selected at random to perform the initial VOC analysis.

Since quantification of ^{14}C required removal of aqueous samples, the ratio of headspace to liquid in the microcosms changed over time. This necessitated a change in

the response factors used to quantify the total amount of VOCs present. The relationship between the volume of liquid and headspace in the serum bottles and the response factors for each VOC was determined using VOC standards. Standards were analyzed on the same day they were prepared, to avoid losses by diffusion through punctures in the septum. Three standard types were prepared: Gas Set #1 (methane, VC, and ethene); Gas Set #2 (acetylene and ethane); and a Liquid Set (TCE and cDCE). The compounds present in the gas sets were chosen to minimize overlaps in closely eluting peaks (Table A.2). For each set, four serum bottles were prepared, each with a different amount of the respective chemical. For gases, the volumes used were 0.025, 0.05, 0.075, and 0.1 mL. Volumes were converted to moles using the Ideal Gas Law. Gases were added to serum bottles containing varying volumes of DDI water (100, 85, 70, and 60 mL), spanning the highest amount present at time-zero and extending to the lowest amount anticipated to remain at the end of the incubation period. Glass beads were added to the bottles to displace the same volume of water as the crushed rock, i.e., ~6 mL. The serum bottles were sealed with Teflon-faced gray butyl septa and aluminum crimp caps. For the liquid set, a stock solution of TCE and cDCE in methanol was prepared gravimetrically. Aliquots (10, 20, 40 and 100 μL) of the stock solution were added to the four serum bottles.

Because Henry's Law Constants are impacted by temperature, it was necessary to determine response factors for each temperature used. The serum bottles were placed and secured in their respective incubator and allowed to reach the target temperature (18, 25, 30, 35, and 40°C), while simultaneously reaching equilibrium. The incubators were secured onto a large shaker table (~120 rpm) (Figure A.4). Once the temperature was

achieved, bottles were removed one at a time and a 0.5 mL gas sample was immediately injected onto the GC. Peak area units were recorded for each injection and then values were plotted against the known amount of each compound in the serum bottles. The slope of this plot yielded the data for calculation of final volume-dependent response factors, shown in Table A.3.

Collecting data at each volume allowed the response factors to be plotted as a function of volume for each temperature. A correlation between volume of liquid in the bottle and response factor was developed, making it possible to determine the response factor for any volume present. A sample of these plots is shown in Figure A.1 and final volume-dependent response factors are shown in Table A.4. It is important to note that VC and acetylene do not have a response factor listed at every temperature because the Henry's Law constant for both compounds is close to 1 through most of the temperature range evaluated, indicating that the response factor will not vary as the ratio of gas to liquid changes.

2.8 First-order modeling

Pseudo first-order rate constants were calculated based on the rate of accumulation of ^{14}C degradation products. The rate constants developed through this modeling process were not normalized to the amount of catalyst (rock and/or biomass) present. Therefore, an assumption of the model was that the amount of catalyst was at steady-state, which is analogous to pseudo first-order reaction kinetics.[38]

The accumulation rate of ^{14}C products was used in a mass balance model for ^{14}C in the microcosms, based on the following equation from Mills et al.[34]

$$\Delta C_{p,i} = C_{l,i-1,a} - C_{l,i-1,a}(e^{-k\,\Delta t}) \quad (2)$$

where $\Delta C_{p,i}$ = the increase in ^{14}C products over the i^{th} interval between sampling events (i = 0 to a maximum of 9); $C_{l,i,a}$ = concentration of ^{14}C products in the aqueous phase after removing the liquid and headspace samples, i.e., the beginning of the i^{th} interval; and Δt is the time between sampling events. It was assumed that Δ_i will be zero at i = 0 (i.e., there is no accumulation of ^{14}C products at time-zero). The accumulated ^{14}C products used to calculate the rate constant was quantified by the amount of activity present in $V_{alkaline}$, which includes both $^{14}CO_2$ and ^{14}C-NSR (converted to dpm/mL).

The effect of adsorption was captured through $C_{l,i,a}$, as follows.

$$C_{l,i,a} = C_{tot,i}\left(\frac{V_{l,i}}{V_{l,i} + V_{g,i} \cdot H_{C,T}}\right)(1 - \alpha_t \cdot t) \quad (3)$$

where $C_{tot,i}$ is the total ^{14}C present in the bottle at time t; $V_{l,i}$ is the volume of liquid present at time t; $V_{g,i}$ is the volume of gas present at time t; $H_{C,T}$ is the dimensionless Henry's Law Constant at temperature T; α_t is the percent adsorbed at time t: and t is the incubation time. $H_{C,T}$ was calculated at each temperature as shown in Equation 2.4.

$$H_{C,T} = \frac{exp\left(\frac{A - B}{273.15 + T}\right)}{R(273.15 + T)} \quad (4)$$

where A and B (11.4 and 4.78E03, respectively, for TCE) are dimensionless Henry's Law parameters for temperature dependence of solubility, T is temperature (°C), and R is the universal gas constant (8.206E-5 $m^3 \cdot atm \cdot K^{-1} \cdot mol^{-1}$).[37,39] Calculated dimensionless Henry's Law constants for each temperature are given in Table A.8.

When adsorption was not included, α_t was set to zero. When a linear process was assumed, the percent adsorption was

$$\alpha_{t,lin} = \left(\frac{Final\ \%\ Adsorbed}{Total\ time}\right) \cdot t \qquad (5)$$

When a non-linear process was assumed, the percent adsorption was estimated as

$$\alpha_{t,NL} = C_1 \times ln(C_2 \times t + 1) \qquad (6)$$

C_1 was adjusted so that the curve for percent adsorption passed through the percentage on the final sampling day (t) and C_2 was set to 0.0041. This form of the equation produced a trend in which adsorption was initially faster than if the trend followed a simple first order rate. MATLAB was used to determine rate constants by minimizing the sum of squared errors between the ^{14}C product prediction and the ^{14}C product measurements over time. Triplicate bottles were fitted simultaneously to obtain a single value for k (i.e., as opposed to determining k for each bottle and then taking the average). Calculations were performed in two stages, with the first stage corresponding to the initial conditions and the second stage to all subsequent data points.

The value of k was iterated in the MATLAB script until a minimum value was obtained for the sums of squares of error determined as the squared difference between the experimental and estimated ^{14}C product values. The MATLAB function that was used for the iterative approach is *lsqcurvefit*, which is a nonlinear curve-fitting solver function that uses the trust-region-reflective algorithm. Confidence intervals (95%) were determined using the MATLAB function *nlparci* with the Jacobian matrix and residual vector determined from *lsqcurvefit*.

A Student's *t*-test was used to determine if a rate constant for a groundwater sample was statistically different from the FSGW control ($\alpha = 0.05$). If it was significant, a net *k* value was calculated by subtracting the FSGW rate. The confidence interval for the net rate constant was determined by propagation of error using standard deviations derived from the confidence intervals.[34]

2.9 Arrhenius constant

For rate constants that followed a consistent trend with temperature, the results were fit to the Arrhenius equation.

$$\ln k = \ln A - \frac{u}{RT} \qquad (7)$$

where *k* is the temperature dependent pseudo-first order rate constant (yr^{-1}), *A* is the pre-exponential factor (a constant for each chemical reaction), *u* is the Arrhenius temperature coefficient (kJ/mol), *R* is the universal gas constant (8.31447E-3 kJ/mol*K), and *T* is the absolute temperature (K). The value of *u* was calculated by plotting data for the natural logarithm of *k* vs 1/T, where the slope is equal to *-u/R*. A positive *u* value indicates that the rate increases as the temperature increases.

The Arrhenius equation is often simplified to provide the relationship between rate constants at two temperatures.

$$k_1 = k_2 \cdot e^{C(T_1 - T_2)} \qquad (8)$$

where k_1 and k_2 are rate constants are temperatures T_1 and T_2 and *C* is defined by equation 2.9.

$$C = \frac{u}{R \cdot T_1 \cdot T_2} \quad (9)$$

The value of C is often expressed in terms of a dimensionless coefficient, θ.

$$C = \ln \theta \quad (10)$$

2.10 Liquid scintillation counting

Beta radiation was detected and quantified using a Tri-Carb 2910 TR (PerkinElmer, Inc.), which is a low activity liquid scintillation counter. The counter utilizes Time-Resolved Liquid Scintillation Counting, which allowed for high sensitivity and low background counting of samples. When setting up sample runs, the quantification interface QuantaSmart™ was used. The assay parameters were set up for single DPM measurements. The instrumental protocol was fixed as shown in Table A.9. Acidic sparged samples, direct headspace samples, and liquid samples taken directly from the serum bottles were counted within 3 h of the sampling event. The sparged alkaline liquid samples were incubated quiescently (in the dark) for approximately 12 h before counting, to reduce chemiluminescence arising from the high pH of the 2.5 mL sample mixed with the LSC.

3.0 RESULTS AND DISCUSSION

3.1 First Order Rate Constants

^{14}C product data for the unamended, lactate-amended, and killed control treatments are shown at all temperatures in Figure 3. In each panel the corresponding results for the FSGW controls are also plotted. Product quantities (in the aqueous phase) are expressed in dpm/mL, thereby normalizing the results to account for volumetric changes to the gas and liquid portions of the microcosms over time due to sampling.

In the unamended microcosms, ^{14}C products accumulated over the first three or four sampling events and then plateaued. The exception was in the 40ºC treatment. After ~50 days of incubation, ^{14}C product accumulation resumed and exceeded the other unamended treatments at the end of the incubation period. The plateau in accumulation suggested that the reductive capacity needed to initiate abiotic transformation was exhausted. Lee and Batchelor[40] measured the reductive capacity for several iron-bearing minerals. The minerals present in the crushed rock are consistent with those typically present in southern Californian sandstone, including iron sulfides, pyrite, fougerite, magnetite, biotite, vermiculite, and quartz. Pyrite and fougerite can play a role in abiotic TCE reduction to acetylene.[5] Reducing power is needed to initiate abiotic reactions such as transformation of TCE (with its carbon at the +2 oxidation state) to chloroacetylene (+0 oxidation state) and acetylene (-2 oxidation state) (Figure 1). As temperature increased, the plateau increased, suggesting that reductive capacity increased with temperature, which is a potentially significant advantage associated with a modest amount of heating.

In the lactate-amended treatments, ^{14}C products accumulated throughout the incubation period. Microbial metabolism of lactate provides a source of electron donor that can restore the reductive capacity of minerals, a process referred to as biologically mediated abiotic degradation (BMAD). In the time frame of these experiments, biotic reductive dechlorination of TCE to cDCE was a minor transformation process (see below), based on a lack of cDCE and VC accumulation in addition to detection of acetylene accumulation. Thus, most of the energy embodied in the lactate was directed at fueling abiotic transformation of TCE. Notably, for the 30, 35, and 40ºC treatments, the rate of product accumulation slowed between days ~40-60. The reason is not known with certainty. However, it is notable that the temperature of the microcosms was adjusted to their targets within several hours of their construction. It is conceivable that the rapid rise in temperature was inhibitory to the ambient microbes. The initial increase in ^{14}C products may have been driven more by exclusively abiotic transformation. Once the microbes adjusted to the higher temperatures, restoration of reductive capacity may have commenced, thereby driving BMAD activity. However, the treatment at 40ºC never caught up to the ones at 30 and 35ºC. This may have been because 40ºC is close to the transition zone between mesophilic and thermophilic, where microbial activity can enter a sharp decline (Figure 2).

The extent of ^{14}C product accumulation in the $HgCl_2$ killed controls was more limited than in the unamended or lactate-amended treatments. This suggests that microbial activity was essential to the abiotic transformation process, including in the unamended treatments. It is unclear if mercury altered the transformation reactions in

some fashion other than inhibiting microbial activity. Autoclaving was considered as an alternative method of stopping biotic processes but was not selected because the use of heat and pressure is known to alter the reactivity of iron minerals that are likely mediating abiotic transformations.

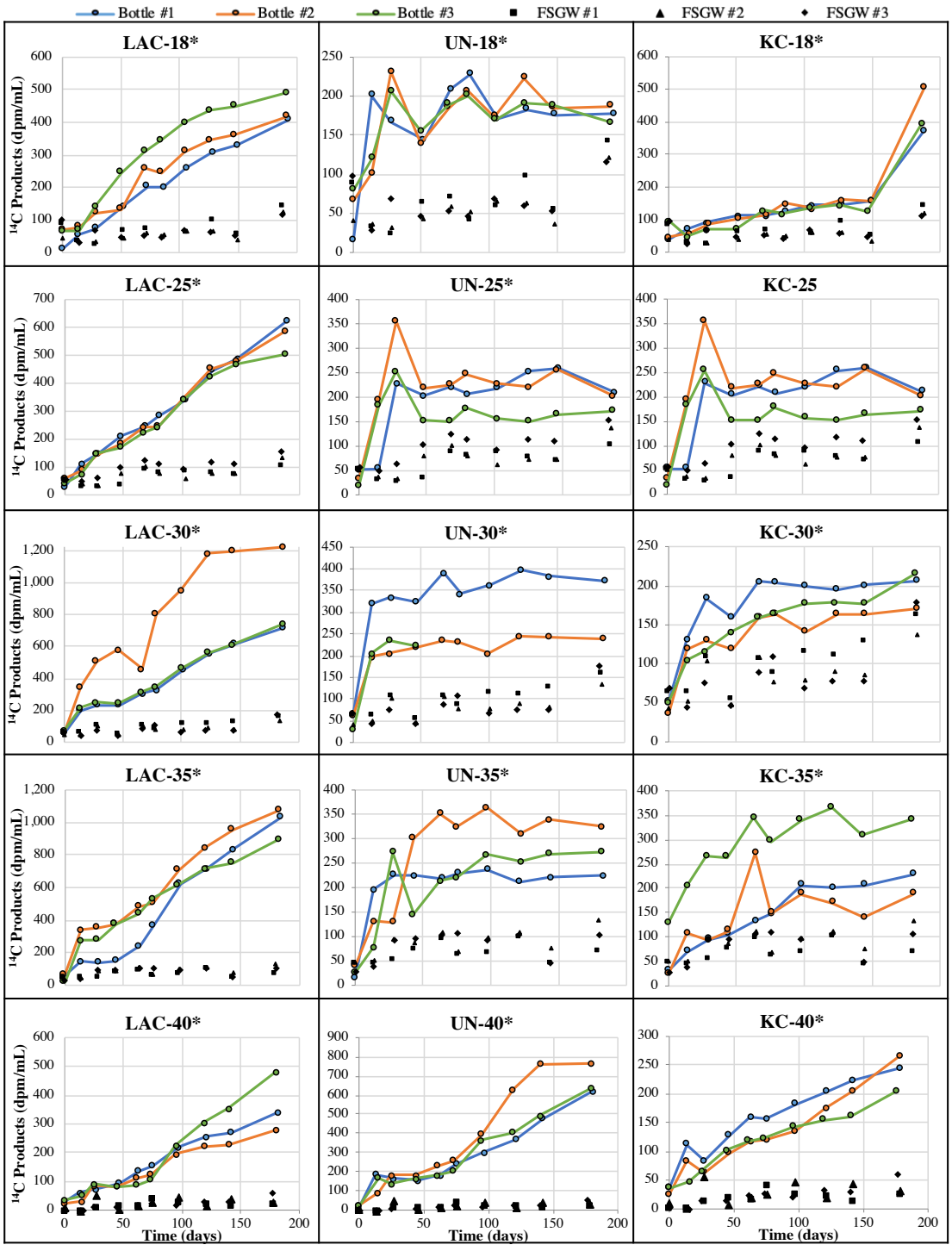

Figure 3. All ^{14}C-labeled products (CO_2 + NSR) for lactate-amended (LAC), unamended (UN), and killed control (KC) treatments at 18, 25, 30, 35, and 40°C (y-axes not identical in scale). * indicates the net rate constant is statistically significant (*p*-value = 0.05).

First order rate constants were estimated initially by using at least the first three data points in Figure 3. The fitting process was repeated by including the first four data points, then five, etc. The highest net rate constant obtained was then selected to represent that treatment. In most cases, the first three data points yielded the highest net rate constant. A summary of the average results is presented in Figure 4 and Table 2 for the case in which adsorption was not included. There are multiple rates listed for FSGW at different sampling times, which corresponds to the number of data points used to determine the net rate constants for each treatment. Results for inclusion of linear and non-linear adsorption are presented in Tables B.2 and B.3. The rate constants were a bit higher when adsorption was included in the mass balance model, but the percent increase was minor (2.6±1.0% for lactate, linear adsorption; 3.2±1.4% for lactate, nonlinear adsorption; 3.2±0.7% for unamended, linear adsorption; 3.8±0.9% for unamended, nonlinear adsorption). Comparisons are shown in Figure B.2.

Figure 5 shows the results for ^{14}C product accumulation results for the three treatments along with the model fits based on k_{net} for the first three sampling events (solid line). It is apparent that including more data points would have resulted in a lower k_{net}, since the model prediction extended beyond the first three sampling events (dashed line) exceeds the observations.

For the unamended treatment, there is a consistent trend in Figure 4 for the rate constant increasing from 18 to 25 to 30ºC, followed by a decrease at 35 and 40ºC. For the lactate-amended treatment, there is no difference in the rate constants at 18 and 25ºC, but a significant increase at 30ºC, followed by a decline at 35 and 40ºC. The peak rate

constants at 30ºC suggest that microbes did not have a chance to adapt to 35 and 40ºC over the time frame of the experiment. This would not likely be a concern in situ, because the rate of heating would be more gradual. Instead, the microcosms used in this research reached their target temperatures in a matter of hours, rather than days.

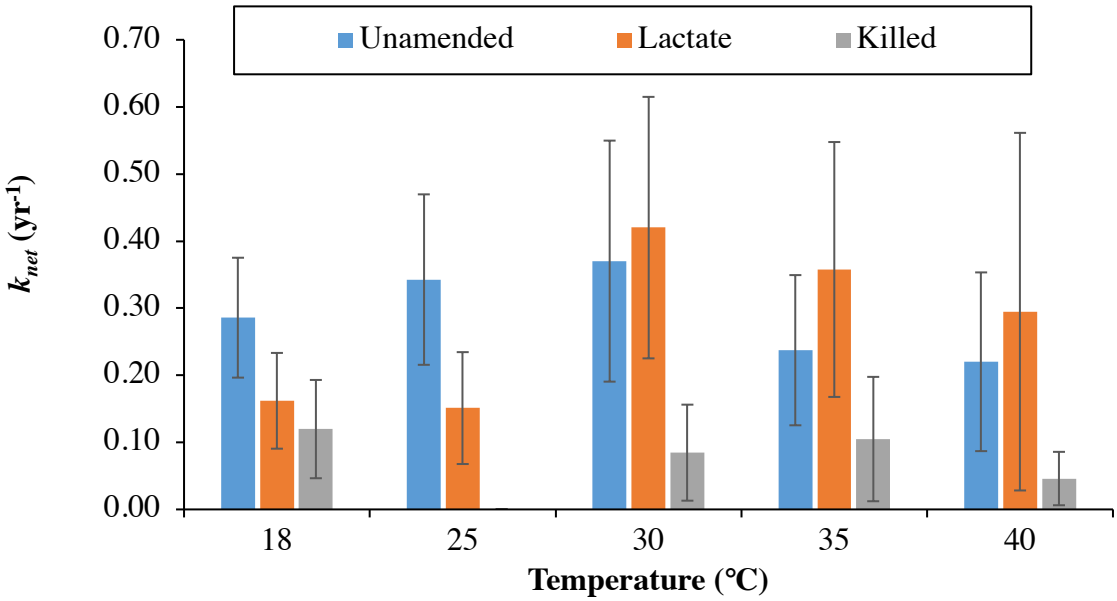

Figure 4. Average pseudo first order rate constants with respective error bars when considering no adsorption and all ^{14}C-labeled products (CO_2 + NSR) for lactate-amended, unamended, and killed control treatments at 18, 25, 30, 35, and 40°C. (n=3 for lactate and unamended; n=3, 4, 4, and 5 for KC at 18, 30, 35, and 40°C, respectively. Error bars (95% confidence intervals) are calculated by propagation of error of the standard deviations of the treatment and respective FSGW, if applicable. If the respective FSGW is not statistically significant, the error is simply the 95% confidence interval for the experimental microcosms.

It would be advisable in future experiments to heat the bottles at a slower rate, on the order of 1-2ºC per day, to give the indigenous population of microbes a chance to adjust. Once the target temperature is reached, the ^{14}C-TCE could be added to assess the rate constants.

Table 2. Maximum net rate values (all^{14}C-products) for lactate-amended, unamended, and killed control treatments at 18, 25, 30, 35, and 40°C when no adsorption is considered.

Treatment	°C	# Data Points	k (yr^{-1})	k_{net} (yr^{-1})	95% CI
Lactate	18	3	1.62E-01	1.62E-01	7.14E-02
	25	3	2.24E-01	1.51E-01	8.34E-02
	30	3	5.75E-01	4.20E-01	1.95E-01
	35	3	4.82E-01	3.58E-01	1.90E-01
	40	3B[a]	5.07E-01	2.95E-01	2.67E-01
Unamended	18	3	2.86E-01	2.86E-01	8.94E-02
	25	3	4.15E-01	3.43E-01	1.27E-01
	30	3	5.25E-01	3.70E-01	1.80E-01
	35	3	3.62E-01	2.37E-01	1.12E-01
	40	3	3.49E-01	2.20E-01	1.33E-01
Killed Control	18	3	1.20E-01	1.20E-01	7.33E-02
	25	NS[b]	NS	NS	NS
	30	4	1.66E-01	8.46E-02	7.16E-02
	35	4	2.04E-01	1.05E-01	9.27E-02
	40	5	1.19E-01	4.60E-02	3.98E-02
FSGW	18	3	NS	-[c]	NS
	25	3	7.26E-02	-	6.99E-02
	30	3	1.55E-01	-	8.04E-02
	30	4	8.19E-02	-	5.08E-02
	35	3	1.24E-01	-	5.66E-02
	35	4	9.90E-02	-	3.12E-02
	40	3	1.29E-01	-	9.55E-02
	40	3B	2.12E-01	-	1.56E-01
	40	5	7.32E-02	-	3.08E-02

[a]3B indicates the 3 data points used in the calculation of the rate constant were the 5-8th sampling event data; [b]NS = not statistically significant; [c]net rates are not applicable to the FSGW treatment.

Unlike the unamended and lactate-amended treatments, temperature had no discernable impact on the rate constants of the killed controls. This observation further suggests that the effect of temperature in the unamended and lactate-amended treatments was primarily through increasing the rate of microbial activity, which in turn was linked

to facilitating the supply of reduced minerals needed to initiate abiotic transformation of TCE.

There is uncertainty whenever pseudo-first order rate constants are compared across studies, since the constants are specific to the experimental conditions (e.g., the type and amount of rock or microbes in relation to the initial concentration of TCE). Nevertheless, Yu et al. [7] evaluated abiotic degradation of TCE with rock and groundwater samples from the same site and used ^{14}C products to determine the rate constants. The microcosms were incubated at ~23ºC, and over a much longer time frame (460 d). The TCE rate constant for the comparable unamended treatment was 0.038 yr^{-1}, an order of magnitude lower than observed in this study at 25ºC (0.34 yr^{-1}). The timeframe likely played a role, based on the decline in the rate constants for this study as sampling was extended beyond several weeks. Although the samples were from the same site, considerable variability in mineral composition is likely from one sample to another.

Given the trends in the pseudo first order rate constants for the unamended and lactate-amended treatments at 18, 25, and 30°C, Arrhenius constants were determined (Tables 3); calculations are shown in Table B.4. It is important to remember that the constant is applicable only to the temperature range embodied in the data, in this case 18-30°C. The values for θ are within the range observed for many kinetic parameters subject to variations in temperature for biological treatment of organic wastes.[41] For many reactions, the rule of thumb is that rates will increase by a factor of 2 for each 10°C increase in temperature, corresponding to a θ of 1.07. The magnitude of increase in rate constants from 18-30°C in this study was 1.3 for unamended and 2.6 for lactate-amended.

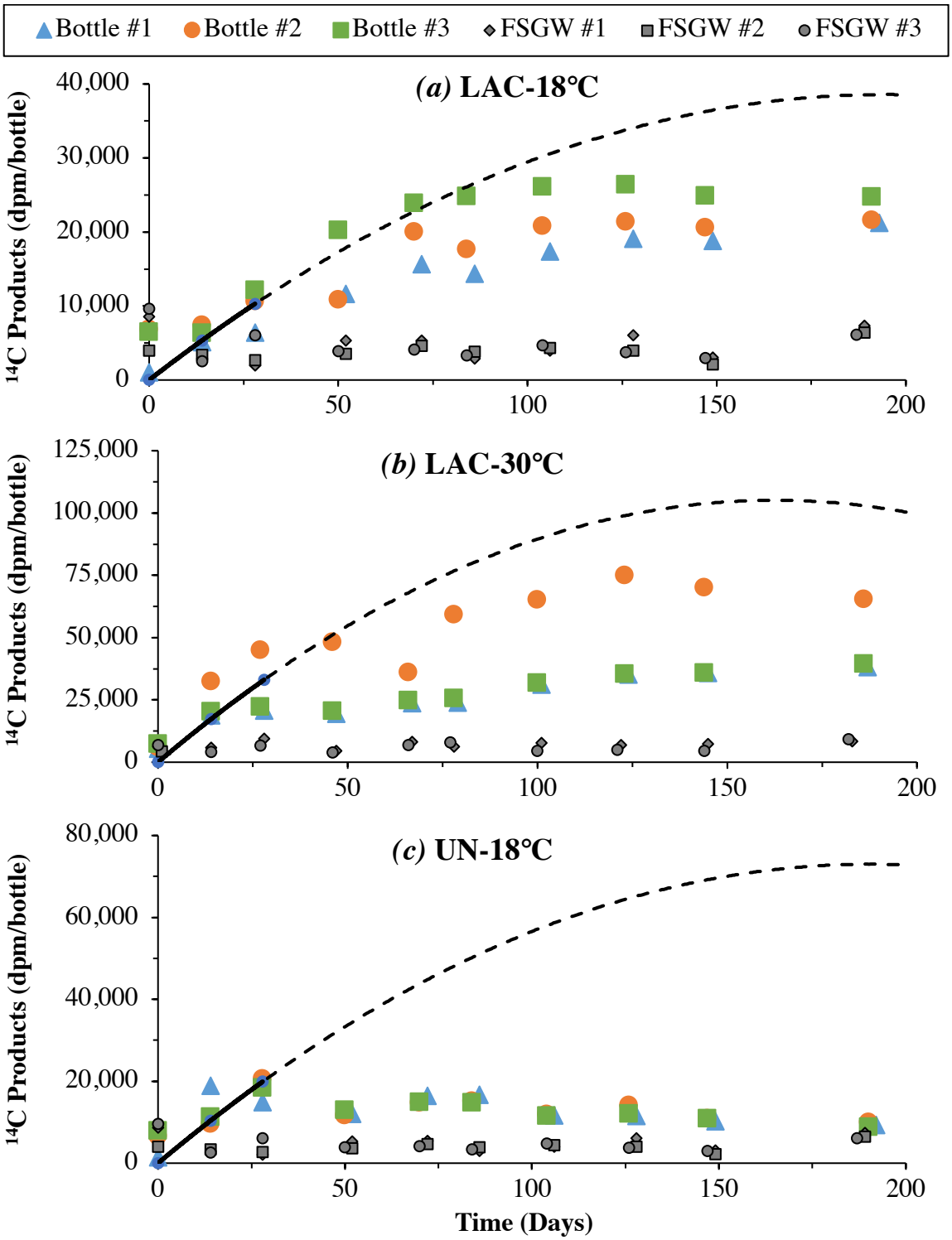

Figure 5. All ^{14}C-labeled products (CO_2 + NSR) for lactate-amended (LAC) treatment at *(a)* 18 and *(b)* 30°C and *(c)* unamended (UN) treatment at 18°C with corresponding model fitting (solid line) and model projection (dashed line).

Table 3. Arrhenius parameters.

	Treatment	
Parameter	**Unamended**	**Lactate-Amended**
u (kJ/mol)	16.02	53.54
C	2.18E-02	7.37E-02
θ	1.02	1.08

3.2 $^{14}CO_2$ and ^{14}C-NSR

The amount of ^{14}C products formed for each sampling point (Figure 3) was determined by alkaline sparging of aqueous samples from the microcosms ($V_{alkaline}$). Using the results from $V_{alkaline}$ and acidic sparging (V_{acidic}), the total products were partitioned into $^{14}CO_2$ and ^{14}C-NSR. Representative results for product accumulation over time are shown in Figure 6 for an unamended and a lactate-amended microcosm. Average results for the distribution of $^{14}CO_2$ and ^{14}C-NSR at the time point used to determine k_{net}, and at the end of the incubation period, are shown in Figure 7. $^{14}CO_2$ predominated in the unamended treatments, while ^{14}C-NSR predominated in the lactate-amended treatments. However, it is important to note that the magnitude of $^{14}CO_2$ was higher in the lactate treatment than the unamended treatment and the ^{14}C-NSR did not increase appreciably over time the way it did in the lactate-amended treatment. Comparison plots for KC and FSGW are included in Appendix B. FSGW and KC had significantly high percentages of ^{14}C-NSR, attributed to the fact that the controls remove microbes and/or minerals which contribute to reactions that produce CO_2.

NSR makes up a large percentage of the total ^{14}C products measured. In this study the NSR was not characterized, however, Darlington et al.[5] identified the

following compounds: glycolate, formate, and acetate. Other compounds were evaluated but not detected, including oxalate, trichloroacetate, glyoxal, glycoaldehyde, and chloroacetate. Presence of these compounds was tested by passing the NSR through an organic acids high performance liquid chromatography column and compared to the peaks which appeared on the UV/vis chromatographs. The NSR compounds present are indicative of a favorable thermodynamics of TCE and cDCE transformation.[5]

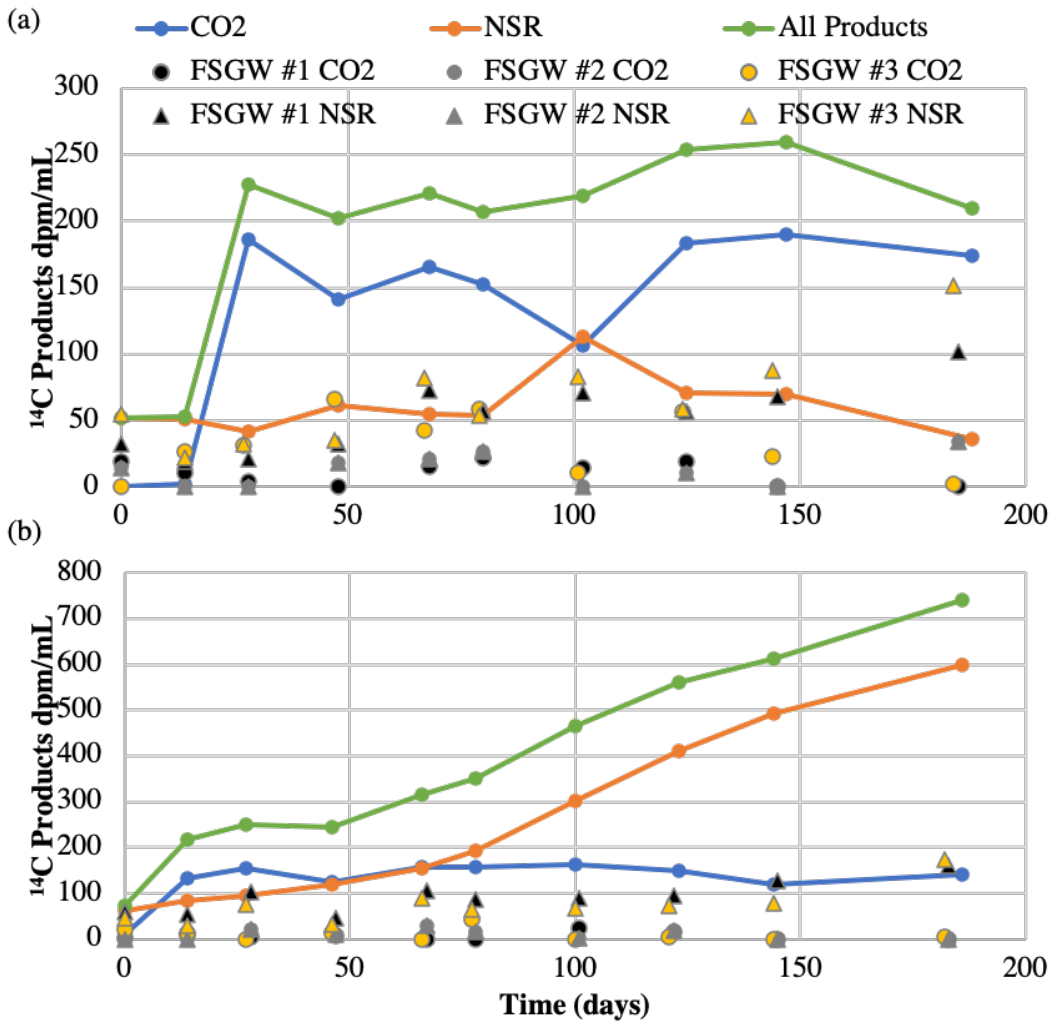

Figure 6. $^{14}CO_2$ and ^{14}C-NSR products recovered over time for (*a*) unamended at 25ºC for microcosms #1 and (*b*) lactate-amended at 30ºC for microcosm #3 and the corresponding FSGW.

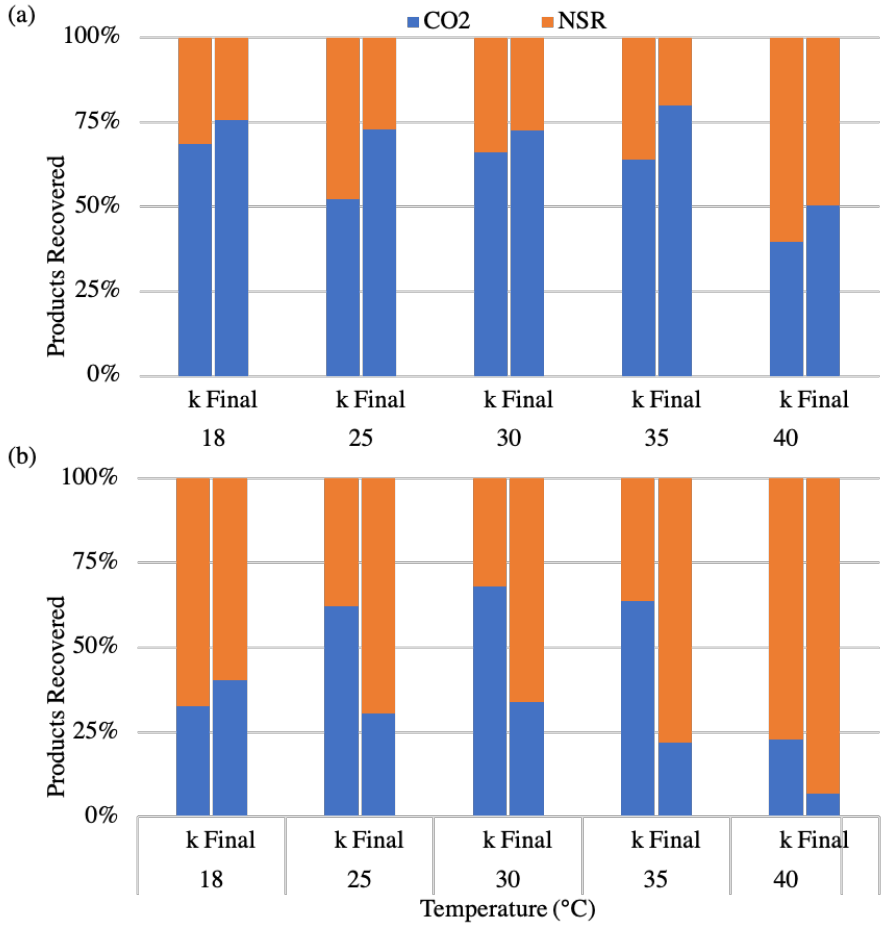

Figure 7. Comparison of $^{14}CO_2$ vs ^{14}C-NSR products recovered for (*a*) unamended and (*b*) lactate-amended treatments at different temperatures. Bars labeled "k" refer to the time point when k_{net} was determined; those labeled "Final" refer to the distribution at the end of the incubation period.

3.3 VOCs

VOC amounts per bottle were measured each time a sample was removed for ^{14}C analysis. Tables 4 and 5 show the results for TCE, cDCE, and methane in the unamended and lactate-amended microcosms, respectively. TCE decreased over the incubation period (~190 d). This decrease is predominately due to physical sample removal but can also be attributed to adsorption to the rock, transformation, and diffusional losses. When

accounting just for physical removal of TCE (Appendix A.8), the final measured amounts were lower, indicating that some of the loss occurred due to adsorption, transformation, and diffusion through the septum.

It is apparent from Tables 4 and 5 that reductive dechlorination was not a dominant pathway in these microcosms, based on the lack of a substantial increase in cDCE over time. cDCE was detected initially, indicating that cDCE was present in the groundwater samples and was not removed simply by flushing the headspace of the microcosm with N_2 after construction of the microcosms.

Low levels (i.e., less than 1% when comparing to initial levels of TCE) of acetylene, ethene, and ethane were periodically detected in the headspace samples (Figure 8), but . Because reductive dechlorination was not a major fate process, the appearance of ethene and ethane was likely attributable to abiotic reduction of acetylene (Figure 1). While it is feasible to determine if these gases were ^{14}C-labeled, that was not assessed with these microcosms. Furthermore, the amount of acetylene, ethene, and ethane in the headspace of the microcosms did not accumulate to a level sufficient to warrant including them as transformation products. By not including these products, the rate constants based on $^{14}CO_2$ and ^{14}C-NSR are likely to be conservative.

Resazurin, which is a colorimetric redox indicator that turns from pink to colorless below an E_h of -110 mV, was added to the groundwater.[7] Potentials below this level are considered conducive to reductive dechlorination of TCE. Addition of resazurin allows for a visual indicator of the redox level in the bottle without having to remove a sample and perform a more complex E_h measurement, which can be unreliable due to the need

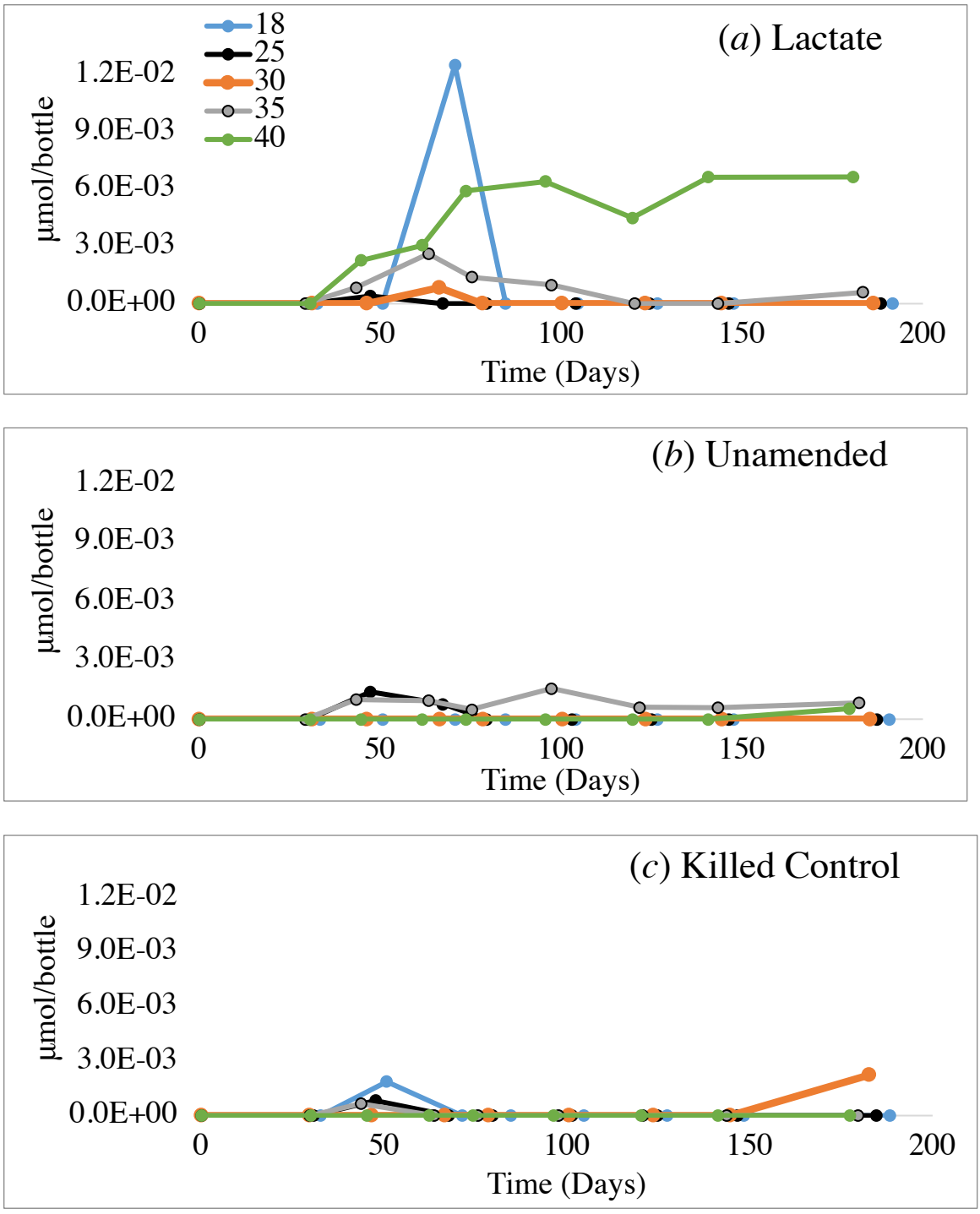

Figure 8. Sum of acetylene, ethene, and ethane amounts in triplicate microcosms with y-axes scaled for comparison.

for a redox couple at equilibrium to have an accurate measurement. Unamended bottles remained light pink through the final day of sampling, further indicating that reductive dechlorination was not the dominant pathway. The majority of lactate-amended microcosms were colorless by the end of incubation, with microcosms at 25, 30, and 35°C reaching colorlessness at approximately 45, 40, and 30 days, respectively, due to addition of electrons lowering the redox potential. Only one of the triplicate lactate-amended bottles at 40°C was colorless by the end of incubation, which is indicative of the high temperature interfering with the microbial activity. FSGW remained purple in color, which agrees with the VOC analysis that cDCE was initially removed from the groundwater through filtering; therefore final cDCE levels were extremely low or non-existent. Killed control microcosms were colorless shortly after the addition of $HgCl_2$.

Based on the amount of lactate added (270 µmol/bottle), the stoichiometric potential methane formation was 405 µmol/bottle. The highest amount formed was only 1% of that potential (Table 5), indicating that methanogenesis was a minor process. Methane levels in the unamended treatments were correspondingly low.

Table 4. Initial and final VOC concentrations in the unamended microcosms.

		VOC (µmol/bottle)					
Compound	**Sample Time**	**18°C**	**25°C**	**30°C**	**35°C**	**40°C**	**Ave**
TCE	Initial	1.8	1.3	0.90	1.1	0.86	1.2
	Final	0.44	0.48	0.28	0.49	0.67	0.47
cDCE	Initial	0.15	0.076	0.074	0.032	0.038	0.073
	Final	0.041	0.045	0.034	0.010	0.035	0.033
Methane	Initial	0.00	0.00	0.00	0.00	0.00	0.00
	Final	0.075	0.048	0.049	0.064	0.070	0.061

Table 5. Initial and final VOC concentrations in the lactate-amended microcosms.

		VOC (µmol/bottle)					
Compound	**Sample Time**	**18°C**	**25°C**	**30°C**	**35°C**	**40°C**	**Ave**
TCE	Initial	1.9	1.3	0.89	0.89	0.76	1.2
	Final	0.50	0.48	0.41	0.32	0.50	0.44
cDCE	Initial	0.16	0.11	0.050	0.008	0.050	0.075
	Final	0.047	0.043	0.049	0.032	0.039	0.042
Methane	Initial	0.00	0.00	0.00	0.00	0.00	0.00
	Final	0.032	4.60	0.042	0.026	0.027	0.94

4.0 CONCLUSIONS

An assay was developed to determine pseudo first order rate constants in microcosms that contain solids and groundwater, based on the rate of accumulation of ^{14}C degradation products from ^{14}C-TCE. The assay was adapted from one developed by Mills et al.[34] to assess co-oxidation of TCE in groundwater alone. Inclusion of crushed rock in this study created a need to consider the impact of adsorption of TCE to the solids. Both linear and non-linear adsorption over time were evaluated. Inclusion of adsorption increased the rate constants, but the magnitude of increase was minor. A different outcome may occur with solids that have a higher adsorption capacity.

When comparing the lactate-amended to unamended treatments at 18, 25, and 30°C, there was greater accumulation of products in the lactate-amended, but still a significant initial rate of accumulation in the unamended bottles. The maximum rate of product accumulation was used to determine net pseudo first order rate constants, which considers the activity in the filter sterilized groundwater controls. The key conclusions are that increasing the temperature from ambient 18°C to 30°C increases degradations rate constants by a factor of 1.3 for the unamended treatment and by 2.6 for the lactate-amended treatment. However, the rate constants trended downward at 35 to 40°C, likely due to the temperature shock associated with the rapid rate of heating at the start of the experiment, which is a problem that can be avoided with in situ thermal acclimation. Adding lactate sustained abiotic degradation of TCE by providing a source of electrons to the reaction taking place. The unamended microcosms lacked a sustainable source of reducing capacity, therefore product accumulation plateaued, rather than steadily

increasing. However, the reductive capacity in the unamended microcosms increased with increasing temperature, a potentially significant advantage to modest heating. The lack of trend and statistical significance in the killed controls confirms the key role of microbial activity in abiotic degradation of TCE.

The results indicate that modest heating of the subsurface is a viable strategy to increase degradation rates and reductive capacity.

APPENDIX A: ADDITIONAL METHODOLOGY DETAILS

A.1 TCE Capture Window and Elution Time

Due to the large number of microcosms needed, this experiment was set up over multiple days with the goal of setting up six microcosms/day. A problem that may occur in this situation is that differences in temperature and barometric pressure affect the ability for accurate GC replication when purifying the ^{14}C-TCE stock solution. In an effort to minimize errors caused by a change in elution time, a standard was created and injected onto the GC at the start of every setup day. This allows for tracking of TCE's elution time over the setup period in addition to easily making adjustments to the capture window. A 160 mL serum bottle was used and 100 mL of DDI and 100 µL of pure, unlabeled TCE were added. The standard was stored upside down on the shaker table. A 0.5 mL gas sample from the headspace was injected onto the GC used for purification while the FID was still in use and the elution time was recorded. The elution time was compared to the elution time recorded on the day that the capture interval was determined. The record of elution times and peak information is shown in Table A.1. It is shown that the capture interval was moved 0.05 minutes earlier on that last day of microcosm setup in an attempt to maximize the amount of ^{14}C-TCE stock delivered.

The capture interval of 0.6 min was chosen based on the rate of flow from the injection needle on the GC and the amount of headspace that was able to be removed to create a negative headspace before ^{14}C-TCE injection to avoid backflow into the GC column. The flow rate was checked every day before microcosm set up to ensure no

significant changes had occurred and acceptable gas flow was maintained. The flow rate remained consistent over the microcosm setup at ~33.5 ± 0.5 mL/min.

Table A.1 TCE elution information recorded when 0.5 mL headspace from TCE DDI standard was injected onto GC used for purification with FID enabled.

Date	Start (min)	Peak (min)	End (min)	Width (min)	PAU[a]	Capture Interval
3/27/19	10.52	10.78	11.12	0.60	6.43	10.15-10.75
3/29/19	10.55	10.78	11.10	0.55	6.42	10.15-10.75
3/30/19	10.53	10.77	11.11	0.58	7.64	10.15-10.75
4/3/19	10.49	10.71	11.07	0.58	7.63	10.10-10.70

[a]PAU = peak area units

Table A.2 Average VOC retention times recorded for each VOC on both GCs during response factor calculations. These values are subject to slight changes depending on physical laboratory conditions.

Compound	Retention Time, (min)	
	GC #1, Greta	GC #2, Ethel
Methane	0.49	0.51
Acetylene	0.71	0.69
Ethene	0.74	0.81
Ethane	0.90	0.93
VC	2.94	3.27
cDCE	7.09	7.08
TCE	10.43	10.27

Table A.3. Response factor data.

		GC #1 (Ethel), V_L (mL/bottle)				GC #2 (Greta) V_L (mL/bottle)			
ºC	**VOC**	**60**	**70**	**85**	**100**	**60**	**70**	**85**	**100**
18	Methane	6.13E-02	5.35E-02	4.68E-02	3.72E-02	5.89E-02	5.16E-02	4.46E-02	3.57E-02
	Acetylene	1.90E-02	1.94E-02	1.98E-02	1.98E-02	1.81E-02	1.84E-02	1.89E-02	1.90E-02
	Ethene	3.35E-02	2.98E-02	2.69E-02	2.26E-02	3.21E-02	2.87E-02	2.56E-02	2.18E-02
	Ethane	1.51E-02	1.36E-02	1.15E-02	9.04E-03	1.55E-02	1.38E-02	1.18E-02	9.40E-03
	VC	5.13E-02	5.12E-02	5.32E-02	5.31E-02	4.88E-02	4.90E-02	5.06E-02	5.09E-02
	cDCE	2.29E-01	2.55E-01	2.92E-01	3.41E-01	2.17E-01	2.44E-01	2.80E-01	3.23E-01
	TCE	1.24E-01	1.33E-01	1.49E-01	1.64E-01	1.16E-01	1.25E-01	1.39E-01	1.54E-01
25	Methane	5.75E-02	5.26E-02	4.36E-02	3.47E-02	5.56E-02	5.09E-02	4.21E-02	3.33E-02
	Acetylene	1.71E-02	1.77E-02	1.69E-02	1.86E-02	1.65E-02	1.69E-02	1.69E-02	1.78E-02
	Ethene	3.18E-02	2.95E-02	2.50E-02	2.08E-02	3.09E-02	2.85E-02	2.41E-02	1.99E-02
	Ethane	1.42E-02	1.27E-02	1.13E-02	9.22E-03	1.45E-02	1.30E-02	1.15E-02	9.43E-03
	VC	4.47E-02	4.55E-02	4.40E-02	4.42E-02	4.30E-02	4.35E-02	4.22E-02	4.25E-02
	cDCE	1.68E-01	1.88E-01	2.20E-01	2.50E-01	1.66E-01	1.82E-01	2.04E-01	2.39E-01
	TCE	9.18E-02	9.95E-02	1.08E-01	1.22E-01	9.04E-02	9.56E-02	1.02E-01	1.13E-01
30	Methane	5.79E-02	5.26E-02	4.42E-02	3.42E-02	5.63E-02	5.11E-02	4.30E-02	3.31E-02
	Acetylene	1.76E-02	1.70E-02	1.72E-02	1.80E-02	1.68E-02	1.63E-02	1.65E-02	1.72E-02
	Ethene	3.12E-02	2.85E-02	2.49E-02	1.99E-02	3.03E-02	2.77E-02	2.43E-02	1.93E-02
	Ethane	1.44E-02	1.33E-02	1.11E-02	8.70E-03	1.48E-02	1.36E-02	1.14E-02	8.89E-03
	VC	4.19E-02	4.16E-02	4.15E-02	3.91E-02	4.01E-02	3.99E-02	3.99E-02	3.73E-02
	cDCE	1.39E-01	1.54E-01	1.83E-01	2.06E-01	1.39E-01	1.54E-01	1.83E-01	2.06E-01
	TCE	8.10E-02	8.45E-02	9.36E-02	1.01E-01	7.57E-02	7.95E-02	8.97E-02	9.00E-02
35	Methane	5.65E-02	5.18E-02	4.33E-02	3.63E-02	5.46E-02	4.98E-02	4.21E-02	3.51E-02
	Acetylene	1.74E-02	1.68E-02	1.68E-02	1.67E-02	1.67E-02	1.62E-02	1.63E-02	1.62E-02
	Ethene	3.15E-02	2.90E-02	2.48E-02	2.17E-02	3.04E-02	2.78E-02	2.39E-02	2.10E-02
	Ethane	1.47E-02	1.33E-02	1.08E-02	8.89E-03	1.52E-02	1.37E-02	1.12E-02	9.18E-03
	VC	4.06E-02	4.14E-02	4.03E-02	4.05E-02	3.90E-02	3.94E-02	3.83E-02	3.95E-02
	cDCE	1.31E-01	1.53E-01	1.76E-01	2.09E-01	1.28E-01	1.45E-01	1.69E-01	1.99E-01
	TCE	7.48E-02	8.24E-02	8.97E-02	9.97E-02	7.09E-02	7.70E-02	8.45E-02	9.44E-02
40	Methane	5.72E-02	5.02E-02	4.15E-02	3.39E-02	5.56E-02	4.96E-02	4.12E-02	3.34E-02
	Acetylene	1.51E-02	1.58E-02	1.47E-02	1.44E-02	3.00E-02	2.98E-02	2.96E-02	2.89E-02
	Ethene	3.05E-02	2.75E-02	2.34E-02	1.97E-02	2.97E-02	2.70E-02	2.32E-02	1.94E-02
	Ethane	1.32E-02	1.22E-02	9.75E-03	8.12E-03	2.82E-02	2.50E-02	2.11E-02	1.74E-02
	VC	3.61E-02	3.54E-02	3.32E-02	3.19E-02	3.53E-02	3.45E-02	3.26E-02	3.15E-02
	cDCE	1.02E-01	1.07E-01	1.19E-01	1.36E-01	9.92E-02	1.07E-01	1.18E-01	1.36E-01
	TCE	6.27E-02	6.28E-02	6.36E-02	6.53E-02	5.94E-02	6.04E-02	6.12E-02	6.51E-02

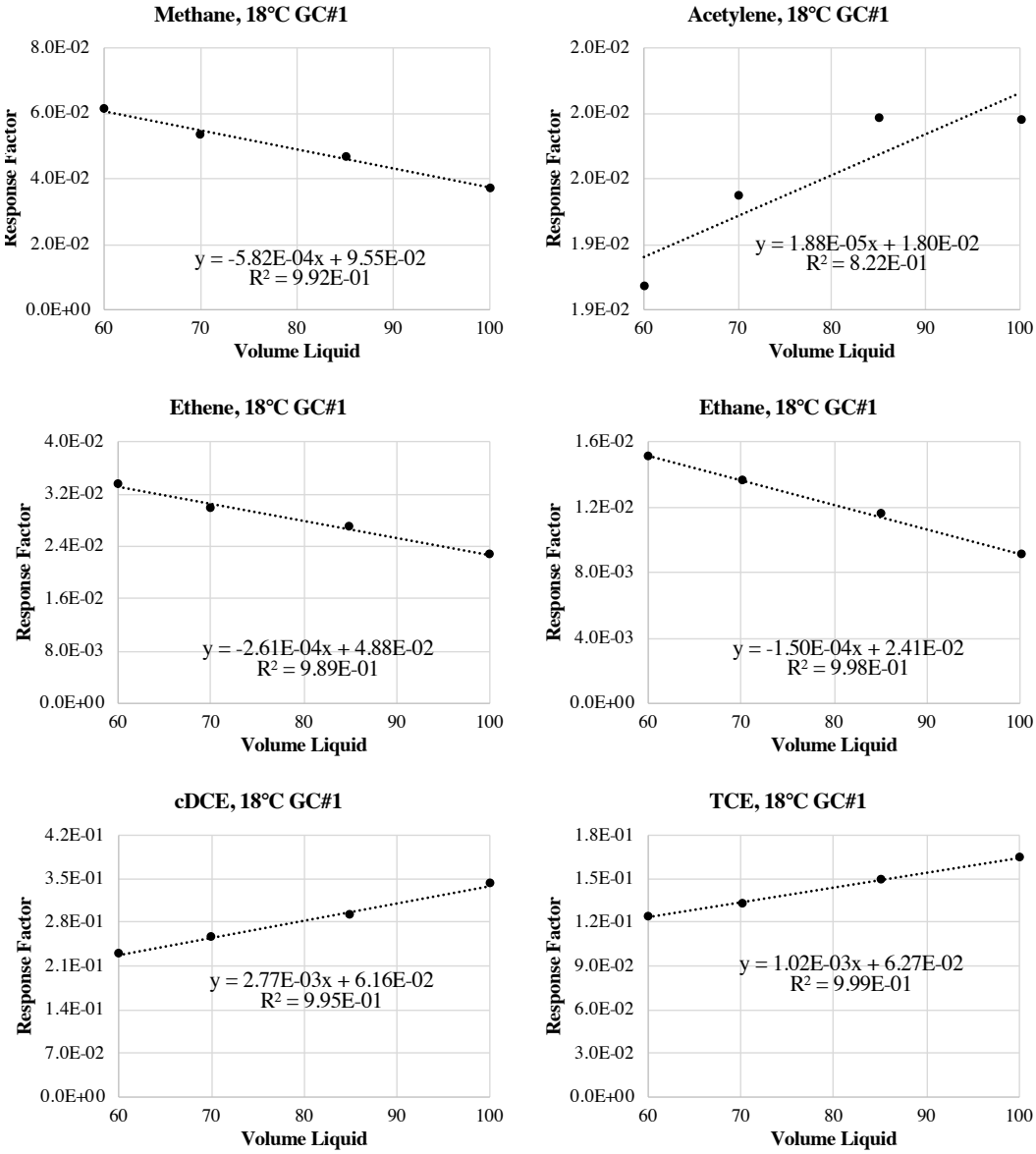

Figure A.1. Response factor vs volume plots for VOCs at 18ºC.

Table A.4. Response factors as a function of volume data for standard equation of a line: y=mx+b, where *y* is the response factor, *m* is the slope, *x* is the volume of liquid (mL), and *b* is the y-intercept.

		GC #1 (Ethel)		GC #2 (Greta)	
(°C)	**VOC**	**slope**	**y int.**	**slope**	**y int.**
18		-5.82E-04	9.55E-02	-5.65E-04	9.22E-02
25		-5.75E-04	9.24E-02	-5.63E-04	8.99E-02
30	Methane	-5.91E-04	9.38E-02	-5.77E-04	9.13E-02
35		-5.13E-04	8.73E-02	-4.91E-04	8.41E-02
40		-5.78E-04	9.12E-02	-5.56E-04	8.87E-02
18		-	-	-	-
25		-	-	-	-
30	Acetylene	-	-	-	-
35		-	-	-	-
40		-	-	-2.73E-05	3.17E-02
18		-2.61E-04	4.88E-02	-2.49E-04	4.67E-02
25		-2.79E-04	4.88E-02	-2.77E-04	4.77E-02
30	Ethene	-2.78E-04	4.80E-02	-2.69E-04	4.66E-02
35		-2.50E-04	4.64E-02	-2.38E-04	4.45E-02
40		-2.69E-04	4.64E-02	-2.57E-04	4.51E-02
18		-1.50E-04	2.41E-02	-1.51E-04	2.46E-02
25		-1.21E-04	2.14E-02	-1.23E-04	2.18E-02
30	Ethane	-1.44E-04	2.33E-02	-1.48E-04	2.38E-02
35		-1.48E-04	2.36E-02	-1.53E-04	2.43E-02
40		-1.31E-04	2.11E-02	-2.67E-04	4.39E-02
18		-	-	5.82E-05	4.52E-02
25		-	-	-	-
30	VC	-	-	-	-
35		-	-	-	-
40		-1.11E-04	4.29E-02	-1.01E-04	4.14E-02
18		2.77E-03	6.16E-02	2.63E-03	5.87E-02
25		2.05E-03	4.49E-02	1.81E-03	5.53E-02
30	cDCE	1.69E-03	3.72E-02	1.69E-03	3.72E-02
35		1.89E-03	1.83E-02	1.77E-03	2.11E-02
40		8.53E-04	4.87E-02	9.09E-04	4.35E-02
18		1.02E-03	6.27E-02	9.51E-04	5.88E-02
25		7.33E-04	4.75E-02	5.48E-04	5.70E-02
30	TCE	5.18E-04	4.93E-02	3.90E-04	5.30E-02
35		6.05E-04	3.90E-02	5.77E-04	3.63E-02
40		6.55E-05	5.84E-02	1.34E-04	5.09E-02

A.2 Percent Moisture and Density Analysis

Percent moisture analysis of the crushed rock was needed in order to determine how much of the ~12g of rock was solid vs. liquid. After microcosms were built, a small sample of soil was removed from the anaerobic chamber and separated into three pre-weighed aluminum trays. The "wet" weight was recorded, and uncovered samples were immediately placed in a 100°C oven to completely dry for 24 hours. Samples were then removed from the oven and immediately placed in a sealed chamber containing Drierite™ pebbles. After trays and contents were completely cooled, trays were quickly removed from the chamber individually and the final "dry" weights were recorded. Percent moisture is calculated using the following equation:

$$\%\ Moisture = \left(1 - \frac{Weight\ of\ Dry\ Soil\ (g)}{Weight\ of\ Wet\ Soil\ (g)}\right) \cdot 100 \qquad (A.1)$$

The average percent moisture was determined to be 84.4 ± 2.6%; data are described in Table A.5.

Table A.5 Percent moisture analysis of crushed rock.

Weight of Wet Rock	Weight of Dry	% Solid	% Moisture
6.8243	5.9374	87.0%	13.0%
4.9284	4.0312	81.8%	18.2%
5.7771	4.8714	84.3%	15.7%

Density of the crushed rock was determined using a simple laboratory method where different volumes of DDI were added to graduated cylinders (triplicates) and a pre-weighed sample of rock is added to each graduated cylinder. The rise in water level was recorded allowing for the increase in water volume to be determined. The density was

determined simply by dividing the mass of rock added (grams) by the volume increase in the graduated cylinder (mL). The triplicate trials were then averaged to give average density of the crushed rock sample, which was equal to 2.10 ± 0.10 g/mL. Data for the density analysis are shown in Table A.6.

Table A.6 Density analysis data of crushed rock.

Weight of Crushed Rock (g)	Starting volume of DDI (mL)	Final Volume of DDI (mL) after rock	Density (g/mL)
11.9168	10	16.00	1.99
12.0008	15	20.55	2.16
12.0000	10	15.55	2.16

A.3 Experimental Sparging Apparatus

Figure A.2 shows the apparatus used when sparging the acid and alkaline samples. The apparatus consists of a supported piece of plywood with 10 air flow meters (Cole-Parmer, 1.4 LPM) connected in parallel by 20 cm thin walled latex rubber tubing (VWR®, 1/16 in. I.D., 3/16 in. wall) which serves at the carrier for N_2 gas. The flow meters allow for control of the flow rate of the gas, which is then directed to sparging needles inserted into the scintillation vials which are vented with disposable needles (BD PrecisionGlideTM, 22 G x 1 1⁄2 in.). Vials are kept on a 30º angle using a custom wooden holder.

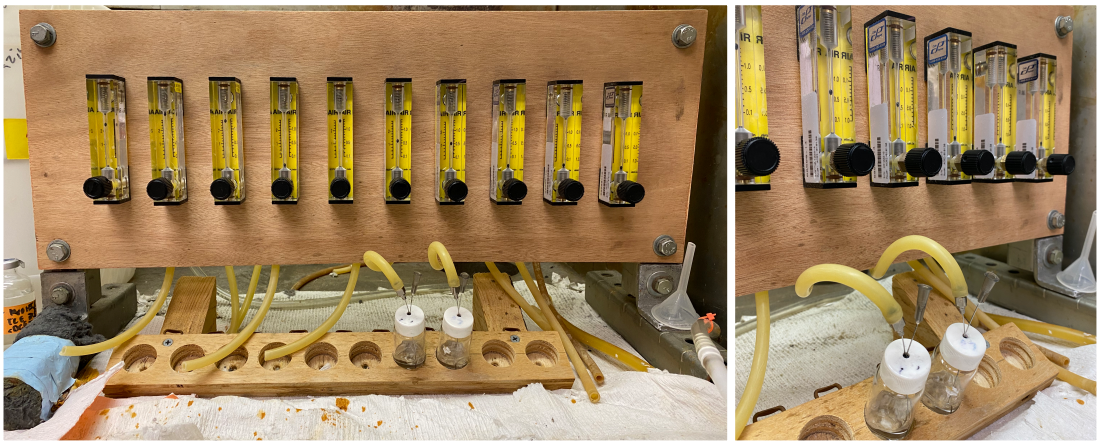

Figure A.2 Sparging apparatus setup depicting sample scintillation vials with sparge and vent needles on the 30º angle wooden holder.

A.4 Incubator Setup

An image of the VWR countertop incubators is shown in Figure A.3. Microcosms were placed upside down in a structured cardboard box to aid in ease of removal, organization, and transportation.

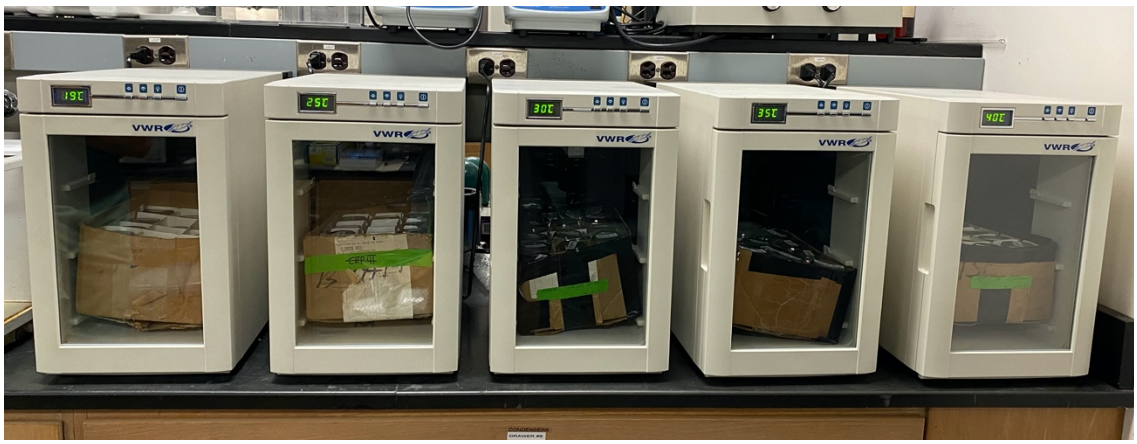

Figure A.3 Incubators setup for each temperature treatment, which can each hold 16 serum bottles (160 mL) stacked in a single layer.

When determining the response factors for VOCs as previously described, incubators needed to be transported to a shaker table where the various standards were wrapped in protective coverings and packed into the incubators with all void space filled with packing material. Microcosms were temporarily removed from incubators for ~ 24hr while response factors were calculated, but no unusual changes in product accumulation were detected. Figure A.4 shows three incubators on the shaker table prior to being packed with material in order to avoid the glass serum bottles potentially breaking while in motion.

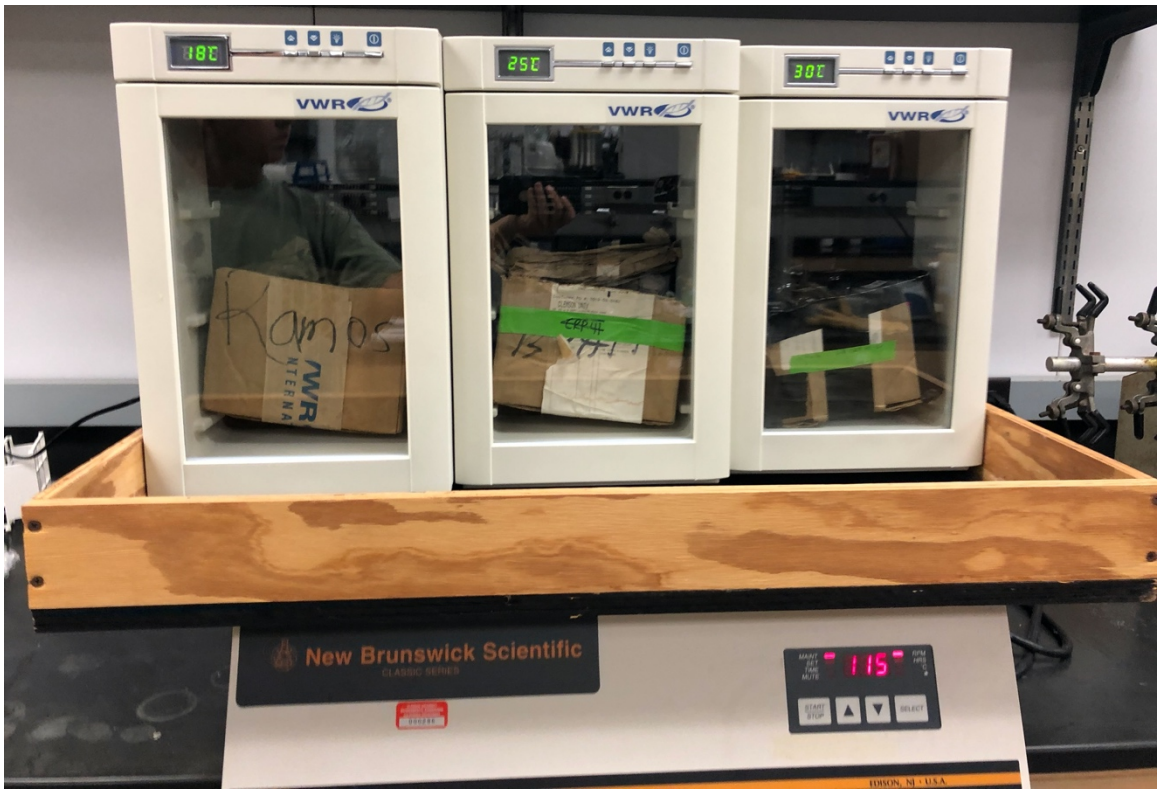

Figure A.4. 18, 25, and 30ºC incubators placed on shaker table in preparation for response factor calculation experiment.

A.5. Percent Adsorbed, Slurry Analysis

Method of the slurry analysis was described in the materials and methods section of this document. Table A.7 gives the final percent adsorbed data for the three treatments at all temperatures. When rates considering adsorption were calculated in Excel and Matlab, individual adsorption data was used which affects the percent aqueous calculation used in both programs. It is important to note the two different types of adsorption considered in this experiment, linear and non-linear. When linear adsorption was used, it was assumed that the adsorption increases uniformly over the time of incubation considered. However, nonlinear adsorption considered a log-based approach to the increase in adsorption, where initially adsorption increased at a faster rate and begins to slow over a function of time. This is shown in Figure A.5, which models adsorption over the first 52 days for the unamended treatment at 18ºC, which had the highest percent adsorption at the end of incubation. Theoretically, the non-linear adsorption would most closely mimic natural conditions, where TCE initially adsorbs quickly to the rock but eventually slows as maximum adsorption capacity is reached. This experiment does not consider back diffusion from rock to groundwater in calculations for adsorption, as this would more likely occur over a longer period of time than the incubation period permitted.[42]

Table A.7 Percent adsorption data for the three crushed rock containing treatments and incubation time when measurements were taken at all temperatures.

Treatment	% Adsorbed	St. Dev	Time (days)
LAC-18	70.63%	4.5%	192
LAC-25	54.60%	9.9%	188
LAC-30	46.92%	7.7%	186
LAC-35	43.09%	4.3%	183
LAC-40	62.91%	8.1%	181
UN-18	90.28%	6.1%	191
UN-25	86.75%	7.4%	187
UN-30	81.31%	10.5%	186
UN-35	83.07%	10.4%	182
UN-40	52.99%	9.3%	180
KC-18	63.77%	9.0%	188
KC-25	65.70%	15.5%	185
KC-30	78.29%	5.5%	183
KC-35	70.79%	11.6%	180
KC-40	69.70%	5.9%	177

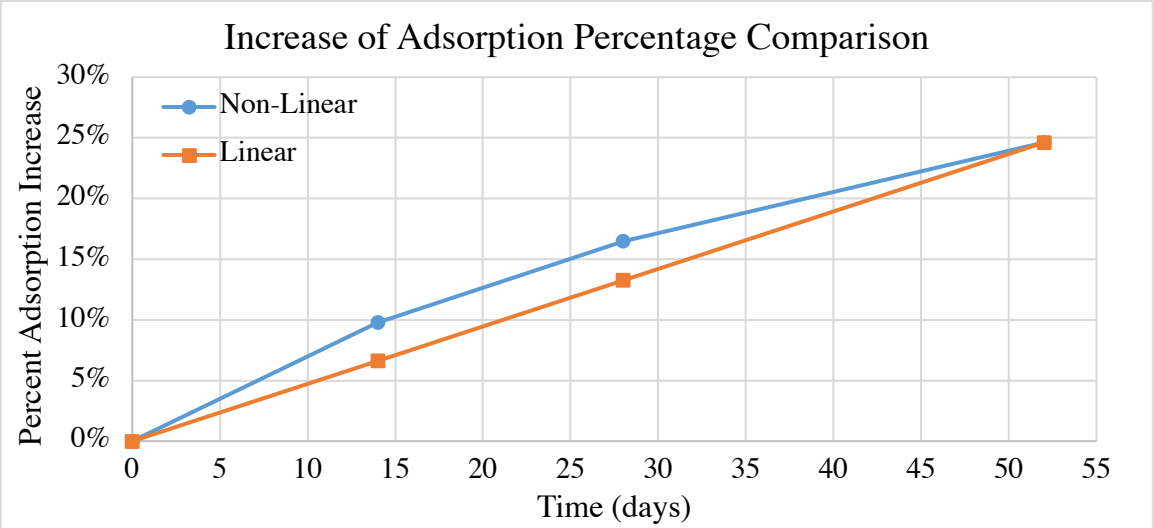

Figure A.5 Comparison of linear vs non-linear adsorption for the unamended treatment at 18ºC.

A.6 TCE Dimensionless Henry's Law Constant vs. Temperature

Due to the temperature dependence of this experiment, it was necessary to take into account the effect of temperature on Henry's Law constant.[43] The calculated Henry's Law constants are shown in Table A.8.

Table A.8. Dimensionless Henry's Law constants for TCE at five target temperatures.

TCE	
Temperature °C	H' dimensionless
18	0.269
25	0.386
30	0.495
35	0.629
40	0.792

A.7 Scintillation Counter Program Setup

Table A.9. Scintillation counter program setup conditions.

Feature	**Setting**
Count Conditions	^{14}C radionuclide
Count Mode	Normal
Quench Set	^{14}C
Quench Indicator	tSIE/AEC
External Standard Terminator	0.5 2s%
Pre-count Delay (min)	0.00
Count Time (min)	15
Assay Count Cycles	1
Repeat Sample Count	1
#Vials/Sample	1
Count Corrections/Special Conditions	Static Controller
Coincidence Time (nsec)	18
Delay Before Burst (nsec)	75

A.8 VOC Estimation based on Physical Removal

VOCs were removed at each sampling event, which can be estimated by multiplying the initial concentration of VOC by the percent mass of VOC remaining at the i^{th} sampling interval (Equations A.2 and A.3).

$$M_{remaining,i} = M_{remaining,i-1} - \sum M_{removed} \quad (A.2)$$

$$M_{removed} = V_{l,removed} \cdot \left(\%\ Aqueous \cdot M_{remaining,i-1}\right) \quad (A.3)$$

where M is the percent mass of VOC and $V_{l,removed}$ is the volume of liquid removed at each sampling event (5.1 mL). The difference in the measured and estimated final concentration values is attributed to adsorption to rock, transformation, and diffusional losses.

APPENDIX B: ADDITIONAL RESULTS

B.1 $^{14}CO_2$ Product Accumulation and Rate Results

Results presented in the body of this document pertained to all ^{14}C products detected, which includes $^{14}CO_2$ and ^{14}C-NSR. Figure B.1 and Table B.1 show results for $^{14}CO_2$ products only. Since not all products are considered in the rate calculations, rates will obviously be lower than when considering all ^{14}C products. The LAC-40 and KC-25 treatment rates become statistically insignificant when only considering $^{14}CO_2$ products. The use of only $^{14}CO_2$ products in the calculation of rate constants tends to be a more conservative approach since it relates the rate constant to a defined degradation product (i.e., CO_2).

Table B.1 Maximum net rate values ($^{14}CO_2$ only) for lactate-amended (LAC), unamended (UN), and killed control (KC) treatments at 18, 25, 30, 35, and 40°C. (-) indicates the net rate coefficient is not statistically significant.

Treatment	(°C)	# Data Points	k_{net} (yr^{-1})	95% Conf.
Lactate	18	4	6.85E-02	4.11E-02
	25	3	1.35E-01	3.84E-02
	30	3	4.20E-01	1.82E-01
	35	3	3.02E-01	1.90E-01
	40	-	-	-
Unamended	18	3	2.03E-01	5.06E-02
	25	3	2.22E-01	9.33E-02
	30	3	3.47E-01	1.05E-01
	35	3	1.91E-01	8.20E-02
	40	3	6.91E-02	5.08E-02
KC	18	-	-	-
	25	-	-	-
	30	3	6.27E-02	2.44E-02
	35	5	3.27E-02	1.72E-02
	40	4	5.32E-02	3.87E-02

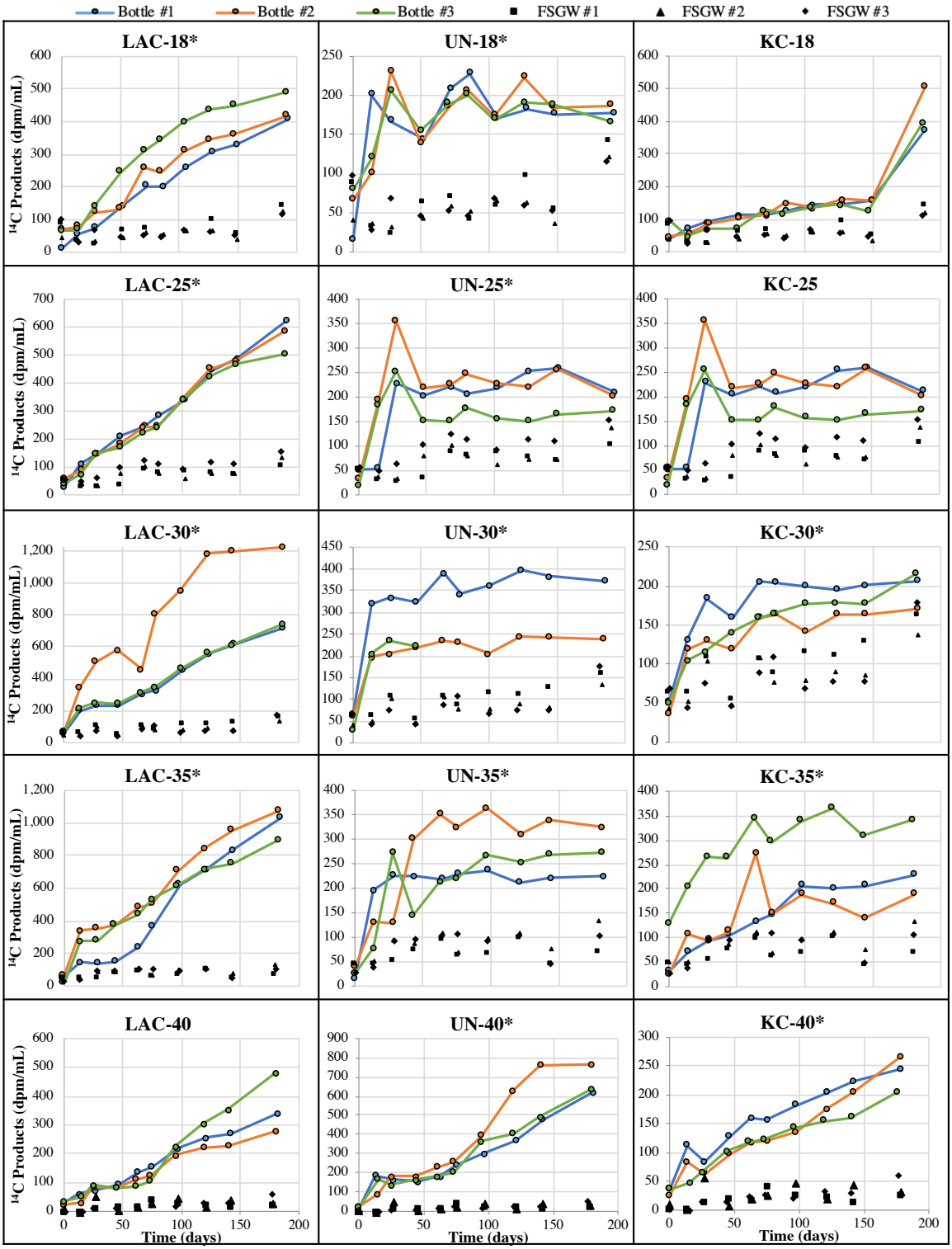

Figure B.1 $^{14}CO_2$ for lactate-amended (LAC), unamended (UN), and killed control (KC) treatments at 18, 25, 30, 35, and 40°C. * indicates the net rate coefficient is statistically significant.

B.2 Additional Adsorption Data

Table B.2 Maximum net rate values (All^{14}C-Products) for lactate-amended (LAC), unamended (UN), and killed control (KC) treatments at 18, 25, 30, 35, and 40°C when linear adsorption is considered. (-) indicates the net rate coefficient is not statistically significant.

Treatment	Temperature	# Data Points	k (yr-1)	knet (yr-1)	95% CI
Lactate	18	3	1.65E-01	1.65E-01	7.26E-02
	25	3	2.27E-01	1.55E-01	8.37E-02
	30	3	5.84E-01	4.28E-01	1.96E-01
	35	3	4.89E-01	3.65E-01	1.91E-01
	40	3B	5.20E-01	3.08E-01	2.70E-01
Unamended	18	3	2.94E-01	2.94E-01	9.03E-02
	25	3	4.25E-01	3.53E-01	1.29E-01
	30	3	5.39E-01	3.84E-01	1.80E-01
	35	3	3.71E-01	2.47E-01	1.13E-01
	40	3	3.55E-01	2.25E-01	1.33E-01
Killed Control	18	3	1.22E-01	1.22E-01	7.44E-02
	25	-	-	-	-
	30	4	1.76E-01	9.45E-02	7.22E-02
	35	3	2.81E-01	1.57E-01	1.56E-01
	40	5	1.28E-01	5.48E-02	4.04E-02
FSGW	18	3	-	-	-
	25	3	7.26E-02	-	6.99E-02
	30	3	1.55E-01	-	8.04E-02
	30	4	8.19E-02	-	5.08E-02
	35	3	1.24E-01	-	5.66E-02
	35	4	9.90E-02	-	3.12E-02
	40	3	1.29E-01	-	9.55E-02
	40	3B	2.12E-01	-	1.56E-01
	40	5	7.32E-02	-	3.08E-02

Table B.3 Maximum net rate values (All^{14}C-Products) for lactate-amended (LAC), unamended (UN), and killed control (KC) treatments at 18, 25, 30, 35, and 40°C when nonlinear adsorption is considered. (-) indicates the net rate coefficient is not statistically significant.

Treatment	°C	# Data Points	k (yr^{-1})	k_{net} (yr^{-1})	95% CI
Lactate	18	3	1.66E-01	1.66E-01	7.28E-02
	25	3	2.28E-01	1.55E-01	8.37E-02
	30	3	5.85E-01	4.30E-01	1.96E-01
	35	3	4.91E-01	3.66E-01	1.91E-01
	40	3B	5.24E-01	3.12E-01	2.71E-01
Unamended	18	3	2.95E-01	2.95E-01	9.05E-02
	25	3	4.27E-01	3.55E-01	1.30E-01
	30	3	5.42E-01	3.87E-01	1.80E-01
	35	3	3.73E-01	2.49E-01	1.13E-01
	40	3	3.56E-01	2.26E-01	1.33E-01
Killed Control	18	3	1.23E-01	1.23E-01	7.46E-02
	25	-	-	-	-
	30	4	1.79E-01	9.74E-02	7.25E-02
	35	3	2.83E-01	1.58E-01	1.57E-01
	40	9	1.03E-01	6.05E-02	2.24E-02
FSGW	18	3	-	-	-
	25	3	7.26E-02	-	6.99E-02
	30	3	1.55E-01	-	8.04E-02
	30	4	8.19E-02	-	5.08E-02
	35	3	1.24E-01	-	5.66E-02
	35	4	9.90E-02	-	3.12E-02
	40	3	1.29E-01	-	9.55E-02
	40	3B	2.12E-01	-	1.56E-01
	40	5	7.32E-02	-	3.08E-02
	40	9	0.042027	-	0.010963

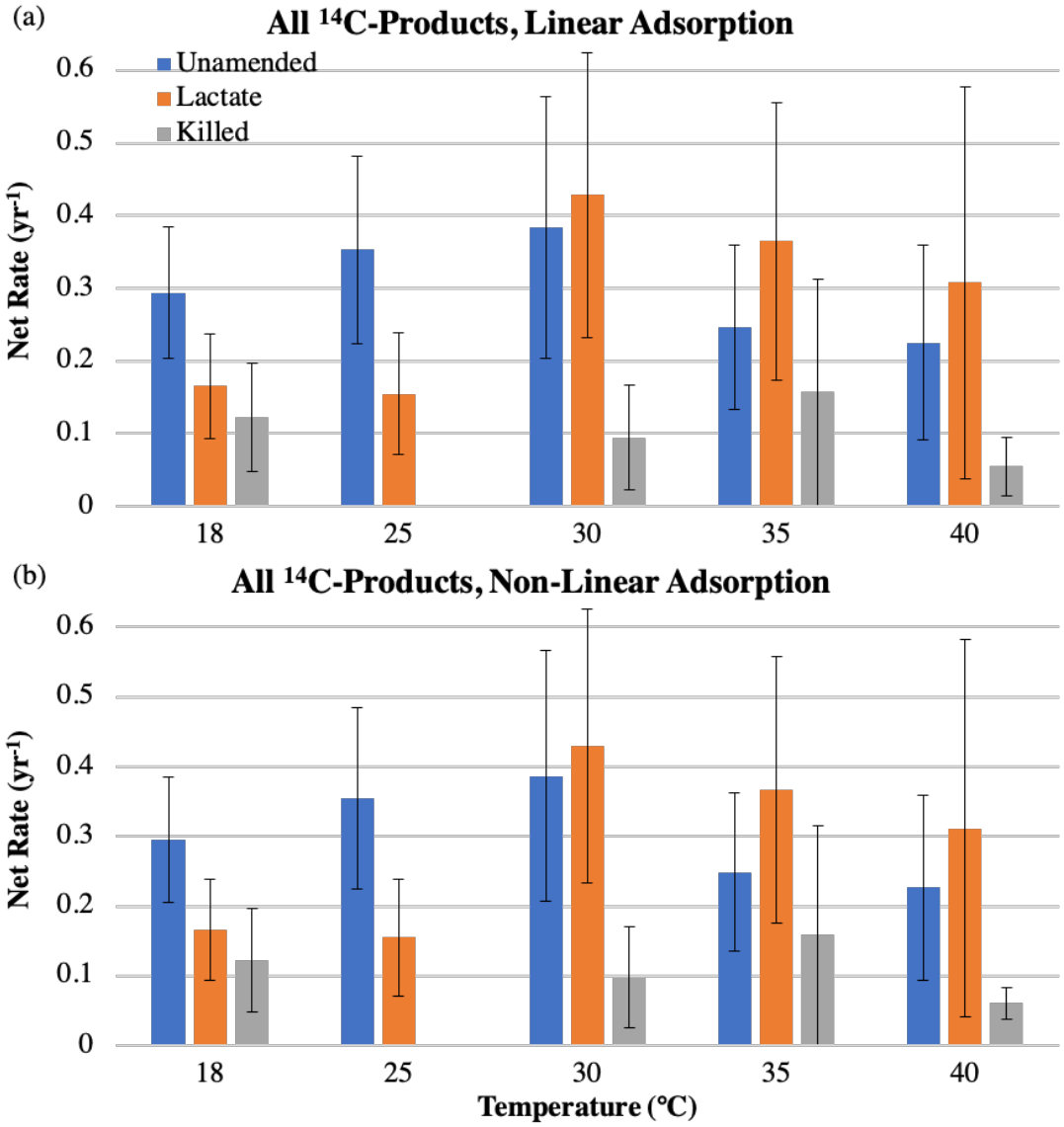

Figure B.2. Comparison of rates considering (*a*) linear adsorption and (*b*) nonlinear adsorption.

B.3 Arrhenius Parameter Calculations

Table B.4. Data and calculations used to find u, C, and θ for lactate-amended (all ^{14}C products, no adsorption considered).

T (°C)	T (K)	1/T	k (yr^{-1})	ln k	Stepwise u (kJ/mol)	ln ($k/k_{25°}$)	$T-T_{25°}$ (K)	Stepwise C	θ
18	291.15	3.43E-03	1.62E-01	-1.82		0.07	-7		
25	298.15	3.35E-03	1.51E-01	-1.89	53.54	0.00	0	7.37E-02	1.08
30	303.15	3.30E-03	4.20E-01	-0.87		1.02	5		

B.4 Additional CO_2 vs. NSR Data

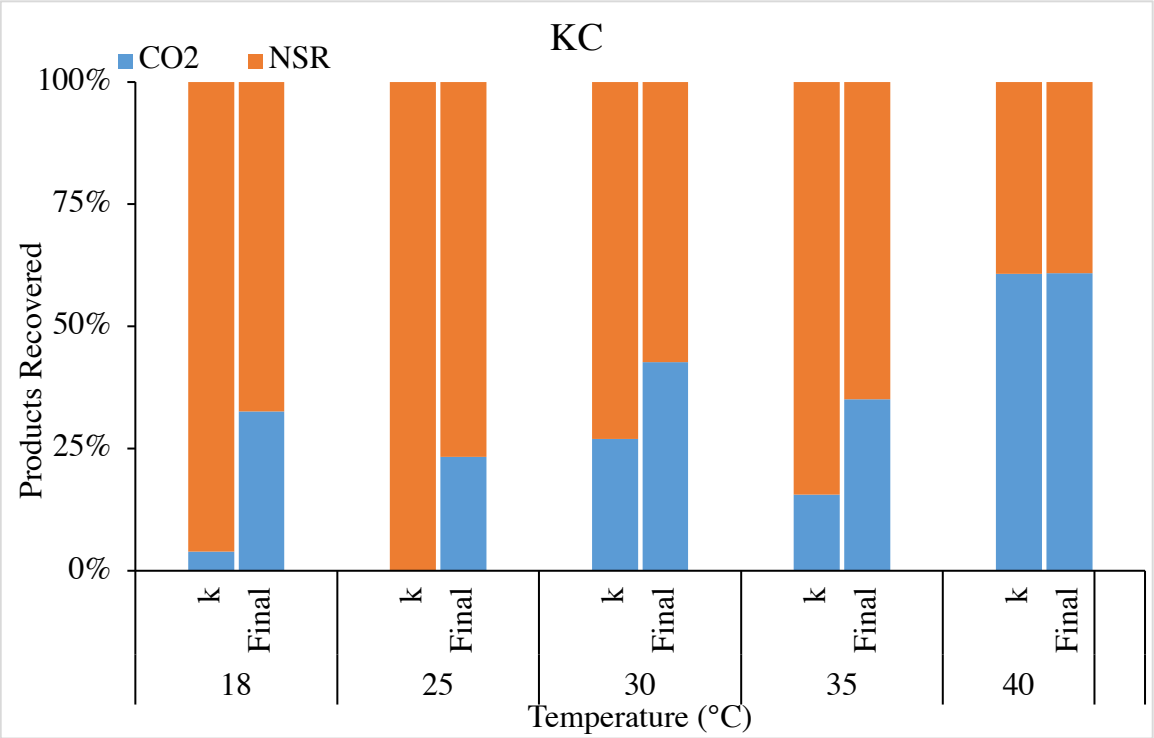

s

Figure B.3. Comparison of $^{14}CO_2$ vs ^{14}C-NSR products recovered for (*a*) killed control and (*b*) FSGW treatments at different temperatures.

B.5 Additional VOC Data

Table B.5. Initial and final VOC concentrations in the killed control microcosms.

		VOC (µmol/bottle)					
Compound	**Sample Time**	**18°C**	**25°C**	**30°C**	**35°C**	**40°C**	**Ave**
TCE	Initial	1.8	1.4	1.1	1.1	0.79	1.2
	Final	0.48	0.47	0.37	0.53	0.66	0.50
	Final, estimated	1.5	1.2	0.88	0.90	0.67	1.0
cDCE	Initial	0.13	0.12	0.088	0.021	0.057	0.082
	Final	0.046	0.045	0.038	0.045	0.043	0.043
	Final, estimated	0.097	0.091	0.068	0.017	0.045	0.064
Methane	Initial	0.00	0.00	0.00	0.00	0.00	0.00
	Final	0.025	0.034	0.020	0.020	0.028	0.025

Table B.6. Initial and final VOC concentrations in the FSGW microcosms.

		VOC (µmol/bottle)					
Compound	**Sample Time**	**18°C**	**25°C**	**30°C**	**35°C**	**40°C**	**Ave**
TCE	Initial	1.7	1.3	1.1	0.84	0.75	1.1
	Final	0.38	0.49	0.49	0.38	0.33	0.41
	Final, estimated	1.4	1.0	0.87	0.70	0.63	0.91
cDCE	Initial	0.12	0.085	0.042	0.000	0.019	0.054
	Final	0.041	0.035	0.030	0.024	0.028	0.032
	Final, estimated	0.093	0.065	0.032	0.000	0.015	0.041
Methane	Initial	0.00	0.00	0.00	0.00	0.00	0.00
	Final	0.012	0.020	0.016	0.016	0.015	0.016

6.0 REFERENCES

(1) Moran, M. J.; Zogorski, J. S.; Squillace, P. J. Chlorinated Solvents in Groundwater of the United States. *Environ. Sci. Technol.* **2007**, *41* (1), 74–81. https://doi.org/10.1021/es061553y.

(2) Wiedemeier, T. H.; Rifai, H. S.; Newell, C. J.; Wilson, J. T. *Natural Attenuation of Fuels and Chlorinated Solvents in the Subsurface*; John Wiley & Sons, Inc.: Hoboken, NJ, USA, 1999. https://doi.org/10.1002/9780470172964.

(3) Oswer X. *Use of Monitored Natural Attenuation at Superfund, RCRA Corrective Action, and Underground Storage Tank Sites ORIGINATING OFFICE*.

(4) Darlington, R.; Lehmicke, L. G.; Andrachek, R. G.; Freedman, D. L. Anaerobic Abiotic Transformations of Cis-1,2-Dichloroethene in Fractured Sandstone. *Chemosphere* **2013**, *90* (8), 2226–2232. https://doi.org/10.1016/j.chemosphere.2012.09.084.

(5) Darlington, R.; Freedman, D. L.; Andrachek, R. G.; Lehmicke, L. Biotic and Abiotic Anaerobic Transformations of Trichloroethene and Cis-1,2-Dichloroethene in Fractured Sandstone. *Environ. Sci. Technol.* **2008**. https://doi.org/10.1021/es702196a.

(6) Yu, R. Laboratory Evaluation of Natural and Enhanced Remediation of Chlorinated Ethenes in Fractured Sandstone, Clemson University, Clemson, SC, 2017.

(7) Yu, R.; Andrachek, R. G.; Lehmicke, L. G.; Freedman, D. L. Remediation of Chlorinated Ethenes in Fractured Sandstone by Natural and Enhanced Biotic and Abiotic Processes: A Crushed Rock Microcosm Study. *Sci. Total Environ.* **2018**, *626*, 497–506. https://doi.org/10.1016/j.scitotenv.2018.01.064.

(8) Arnold, W. A.; Roberts, A. L. Pathways and Kinetics of Chlorinated Ethylene and Chlorinated Acetylene Reaction with Fe(0) Particles. *Environ. Sci. Technol.* **2000**, *34*, 1794–1805.

(9) Adrian, L., Löffler, F. E. *No TitleOrganohalide-Respiring Bacteria*; Springer, Berlin, 2016.

(10) Akob, D.M., Sutton, J.M., Fierst, J.L., Haase, K.B., Baesman, S., Luther, I.I.I.G.W., Miller, L.G., Oremland, R. S. Acetylenotrophy: A Hidden but Ubiquitous Microbial Metabolism. *FEMS Microbio. Ecol.* **2018**, *94*, 1–14.

(11) Arnold, W. A.; Roberts, A. L. *Pathways of Chlorinated Ethylene and Chlorinated Acetylene Reaction with Zn(0)*; 1998.

(12) Stiber, N. A.; Pantazidou, M.; Small, M. J. Embedding Expert Knowledge in a Decision Model: Evaluating Natural Attenuation at TCE Sites. *J. Hazard. Mater.* **2004**, *110* (1–3), 151–160. https://doi.org/10.1016/j.jhazmat.2004.02.048.

(13) Friis, A. K.; Heimann, A. C.; Jakobsen, R.; Albrechtsen, H. J.; Cox, E.; Bjerg, P. L. Temperature Dependence of Anaerobic TCE-Dechlorination in a Highly Enriched Dehalococcoides-Containing Culture. *Water Res.* **2007**. https://doi.org/10.1016/j.watres.2006.09.026.

(14) Löffler, F. E.; Ritalahti, K. M.; Zinder, S. H. Dehalococcoides and Reductive Dechlorination of Chlorinated Solvents. In *Bioaugmentation for Groundwater Remediation*; 2013. https://doi.org/10.1007/978-1-4614-4115-1_2.

(15) Yang, Y.; Higgins, S. A.; Yan, J.; Şimşir, B.; Chourey, K.; Iyer, R.; Hettich, R. L.; Baldwin, B.; Ogles, D. M.; Löffler, F. E. Grape Pomace Compost Harbors Organohalide-Respiring Dehalogenimonas Species with Novel Reductive Dehalogenase Genes. *ISME J.* **2017**, *11* (12), 2767–2780. https://doi.org/10.1038/ismej.2017.127.

(16) Key, T. A.; Richmond, D. P.; Bowman, K. S.; Cho, Y.-J.; Chun, J.; da Costa, M. S.; Rainey, F. A.; Moe, W. M. Genome Sequence of the Organohalide-Respiring Dehalogenimonas Alkenigignens Type Strain (IP3-3T). *Stand. Genomic Sci.* **2016**, *11* (1), 44. https://doi.org/10.1186/s40793-016-0165-7.

(17) Hu, M.; Zhang, Y.; Liu, Y.; Wang, X.; Wong, P. K. Effect of Different Nutrients on the Anaerobic Degradation of Trichloroethene at Optimal Temperature. *Int. Biodeterior. Biodegrad.* **2013**, *85*, 103–107. https://doi.org/10.1016/j.ibiod.2013.06.008.

(18) Freedman, D. L.; Gossett, J. M. *Biological Reductive Dechlorination of Tetrachloroethylene and Trichloroethylene to Ethylene under Methanogenic Conditions*; 1989; Vol. 55.

(19) Lu, X.-X.; Li, G.-H.; Tao, S.; Bosma, T.; Gerritse, J. VOLATILE FATTY ACIDS AS ELECTRON DONORS FOR THE REDUCTIVE DECHLORINATION OF CHLOROETHENES. *J. Environ. Sci. Heal. Part A* **2002**, *37* (4), 439–449. https://doi.org/10.1081/ESE-120003226.

(20) Schöllhorn, A.; Savary, C.; Stucki, G.; Hanselmann, K. W. Comparison of Different Substrates for the Fast Reductive Dechlorination of Trichloroethene under Groundwater Conditions. *Water Res.* **1997**, *31* (6), 1275–1282. https://doi.org/10.1016/S0043-1354(96)00130-3.

(21) Lee, I.-S.; Bae, J.-H.; Yang, Y.; McCarty, P. L. Simulated and Experimental Evaluation of Factors Affecting the Rate and Extent of Reductive Dehalogenation

of Chloroethenes with Glucose. *J. Contam. Hydrol.* **2004**, *74* (1–4), 313–331. https://doi.org/10.1016/j.jconhyd.2004.03.006.

(22) Kosegi, J. M.; Minsker, B. S.; Dougherty, D. E. Feasibility Study of Thermal In Situ Bioremediation. *J. Environ. Eng.* **2000**, *126* (7), 601–610. https://doi.org/10.1061/(ASCE)0733-9372(2000)126:7(601).

(23) Heron, G.; Baker, R. S.; Bierschenk, J. M.; Lachance, J. C. *Heat It All the Way – Mechanisms and Results Achieved Using In-Situ Thermal Remediation*.

(24) Temperature and Microbial Growth.

(25) Bradley, P. M. History and Ecology of Chloroethene Biodegradation: A Review. *Bioremediat. J.* **2003**, *7* (2), 81–109. https://doi.org/10.1080/10889860390246141.

(26) Ritalahti, K. M.; Amos, B. K.; Sung, Y.; Wu, Q.; Koenigsberg, S. S.; Löffler, F. E. Quantitative PCR Targeting 16S RRNA and Reductive Dehalogenase Genes Simultaneously Monitors Multiple Dehalococcoides Strains. *Appl. Environ. Microbiol.* **2006**, *72* (4), 2765–2774. https://doi.org/10.1128/AEM.72.4.2765-2774.2006.

(27) Sherwood Lollar, B.; Slater, G. F.; Sleep, B.; Witt, M.; Klecka, G. M.; Harkness, M.; Spivack, J. Stable Carbon Isotope Evidence for Intrinsic Bioremediation of Tetrachloroethene and Trichloroethene at Area 6, Dover Air Force Base. *Environ. Sci. Technol.* **2000**, *35* (2), 261–269. https://doi.org/10.1021/ES001227X.

(28) Morrill, P. L.; Lacrampe-Couloume, G.; Slater, G. F.; Sleep, B. E.; Edwards, E. A.; McMaster, M. L.; Major, D. W.; Sherwood Lollar, B. Quantifying Chlorinated Ethene Degradation during Reductive Dechlorination at Kelly AFB Using Stable Carbon Isotopes. *J. Contam. Hydrol.* **2005**, *76* (3–4), 279–293. https://doi.org/10.1016/j.jconhyd.2004.11.002.

(29) Illman, W. A.; Alvarez, P. J. Performance Assessment of Bioremediation and Natural Attenuation. *Crit. Rev. Environ. Sci. Technol.* **2009**, *39* (4), 209–270. https://doi.org/10.1080/10643380701413385.

(30) Alvarez, P. J. J.; Illman, W. A. *Bioremediation and Natural Attenuation: Process Fundamentals and Mathematical Models*; John Wiley & Sons, Inc.: Hoboken, NJ, 2006.

(31) Anderson, T. A.; Walton, B. T. Comparative Fate of [^{14} C]Trichloroethylene in the Root Zone of Plants from a Former Solvent Disposal Site. *Environ. Toxicol. Chem.* **1995**, *14* (12), 2041–2047. https://doi.org/10.1002/etc.5620141206.

(32) Chokejaroenrat, C.; Kananizadeh, N.; Sakulthaew, C.; Comfort, S.; Li, Y.

Improving the Sweeping Efficiency of Permanganate into Low Permeable Zones to Treat TCE: Experimental Results and Model Development. *Environ. Sci. Technol.* **2013**, *47* (22), 13031–13038. https://doi.org/10.1021/es403150x.

(33) Darlington, R., Lehmicke, L., Andrachek, R. G. Biotic and Abiotic Anaerobic Transformations of Trichloroethene and Cis-1,2-Dichloroethene in Fractured Sandstone. *Environ. Sci. Technol.* **2008**, *42*, 4323–4330.

(34) Mills, J. C.; Wilson, J. T.; Wilson, B. H.; Wiedemeier, T. H.; Freedman, D. L. Quantification of TCE Co-Oxidation in Groundwater Using a 14C–Assay. *Groundw. Monit. Remediat.* **2018**. https://doi.org/10.1111/gwmr.12266.

(35) Pierce, A. A. Isotopic and Hydrogeochemical Investigation of Major Ion Origin and Trichloroethene Degradation in Fractured Sandstone., 2005.

(36) Schaefer, C. E.; Towne, R. M.; Lippincott, D. R.; Lazouskaya, V.; Fischer, T. B.; Bishop, M. E.; Dong, H. Coupled Diffusion and Abiotic Reaction of Trichlorethene in Minimally Disturbed Rock Matrices. *Environ. Sci. Technol.* **2013**, *47* (9), 4291–4298. https://doi.org/10.1021/es400457s.

(37) Gossett, J. M. Measurement of Henry's Law Constants for C1 and C2 Chlorinated Hydrocarbons. *Environ. Sci. Technol.* **1987**, *21* (2), 202–208. https://doi.org/10.1021/es00156a012.

(38) Schmidt, S. K.; Simkins, S.; Alexander, M. Models for the Kinetics of Biodegradation of Organic Compounds Not Supporting Growth. *Appl. Environ. Microbiol.* **1985**, *50* (2), 323–331.

(39) Sander, R. Compilation of Henry's Law Constants (Version 4.0) for Water as Solvent. *Atmos. Chem. Phys* **2015**, *15*, 4399–4981. https://doi.org/10.5194/acp-15-4399-2015.

(40) Lee, W.; Batchelor, B. Reductive Capacity of Natural Reductants. *Environ. Sci. Technol.* **2003**, *37* (3), 535–541. https://doi.org/10.1021/es025830m.

(41) Grady, C. P. L.; Daigger, G. T.; Love, N. G.; Filipe, C. D. M. *Biological Wastewater Treatment: Third Edition*; IWA Publishing, 2011.

(42) Chapman, S. W.; Parker, B. L. Plume Persistence Due to Aquitard Back Diffusion Following Dense Nonaqueous Phase Liquid Source Removal or Isolation. *Water Resour. Res.* **2005**, *41* (12), 1–16. https://doi.org/10.1029/2005WR004224.

(43) Schwarzenbach, R. P.; Gschwend, P. M.; Imboden, D. M. *Environmental Organic Chemistry, 3rd Edition*; 2016.